Postprint of: Makoś-Chełstowska P., Słupek E., Kramarz A., Dobrzyniewski D., Szulczyński B., Gębicki J., Green monoterpenes based deep eutectic solvents for effective BTEX absorption from biogas, CHEMICAL ENGINEERING RESEARCH & DESIGN Vol. 188 (2022), pp.179-196, DOI: 10.1016/j.cherd.2022.09.047

Green monoterpenes based deep eutectic solvents for effective BTEX absorption from biogas

Patrycja Makoś-Chełstowska[1,2]*, Edyta Słupek[1], Aleksandra Kramarz[1], Dominik Dobrzyniewski[1], Bartosz Szulczyński[1] and Jacek Gębicki[1]

[1] Department of Process Engineering and Chemical Technology, Faculty of Chemistry, Gdansk University of Technology, 80-233 Gdansk, Poland

[2] EcoTech Center, Gdańsk University of Technology, 80-233 Gdańsk, Poland

ABSTRACT:

The combustion of biogas which contains significant amounts of monoaromatic hydrocarbons, i.e. benzene, ethylbenzene, toluene, and xylene (BTEX) can cause many technological, environmental, and health problems. Therefore, in these studies, a new physical absorption method based on deep eutectic solvents (DES) consisting of monoterpenes and carboxylic acids was developed for BTEX removal. A total of 39 DES were synthesized, of which seven were selected based on their affinity to BTEX, favorable physicochemical properties, and "green" character. Detailed structural (i.e. ^{1}H NMR, ^{13}C NMR, and FT-IR) and physicochemical experiments (i.e. melting point, density, viscosity, and surface tension) were performed for the DES. Then, DESs were used for the absorption process in both the laboratory and enlarged scale. BTEX absorption was monitored using two methods, including "in-situ" gas chromatography, and "online" sensors matrices. The crucial absorption

parameters i.e. type of DES, temperature, and regeneration possibility were carefully studied. The mechanism of BTEX absorption was explained using experimental spectroscopic techniques and theoretical analysis based on the COSMO-RS model. The obtained results indicate that Eucalyptol:Octanoic acid can selectively capture BTEX from a biogas mixture due to the formation of electrostatic interaction. DES absorption capacity is 53.96 mg/g, which is comparable with commercially available absorbents.

KEYWORDS: monoterpenes, monoaromatic hydrocarobons, BTEX, biogas, absorption, deep eutectic solvents

1. INTRODUCTION

Currently, an increase in demand for renewable energy production from natural sources can be observed. This is due to a number of factors, including the introduction of increasingly stringent climate policies limiting coal mining or assuming a phase-out of nuclear power plants, as well as the current war-induced fuel crisis. Therefore, more and more countries are considering the use of biogas from waste materials as renewable energy that could make countries less dependent on energy imports. The main problem in the widespread use of biogas is the presence of large amounts of organic and inorganic pollutants. Till now, many methods have been developed to purify biogas from inorganic substances, but there are still few technologies dedicated to the removal of volatile organic compounds from the biogas stream. One of the groups of problematic substances in biogas is monoarmomatic hydrocarbons including benzene, toluene, ethylbenzene, and xylenes (BTEX). These compounds are also one of the most common chemical pollutants of air, natural, and waste

gasses [1,2]. The presence of BTEX in biogas streams is mainly caused by the volatilization of intermediate products formed during fermentation processes. The concentration of BTEX in biogas streams can vary significantly depending on the raw material used in the fermentation process. Nevertheless, the concentration may vary from 94 to 1906 mg/m^3 [3]. The presence of BTEX in biogas streams is unfavorable from ecological, public health, and industrial point of view [4,5]. Most of BTEX have a confirmed carcinogenic potential and adverse effects on the water and air environment [6–8]. In addition, combustion of biogas containing high concentrations of BTEX can cause corrosion, contamination, and clogging of engine systems [9,10]. Therefore, it is essential to remove monoaromatic hydrocarbons from biogas streams.

Currently, in the literature, we can find several methods dedicated to the removal of BTEX from biogas, including: absorption, catalytic oxidation, conventional adsorption, pressure swing adsorption, thermal swing adsorption, membrane, biological, and cryogenic methods [11–16]. Nevertheless, some of these methods show only low BTEX removal efficiency, long-time operation, require the use of toxic organic solvents, high capital investment, and running costs [17]. Therefore, the development of a cost-effective, efficient, "green" technology for BTEX removal from biogas streams is a major challenge for the energy industry. One of the most widely used industrial technology for volatile organic compounds (VOCs) captured from biogas is physical absorption. Physical scrubbing has some pros, including low operation and investment cost, good efficiency, and can be considered environmentally friendly if appropriate absorbents are used [18]. Among the available absorbents, the following can be distinguished triethylene glycol [19], fluorocarbon surfactants [20], polyethylene glycol, paraffin, water emulsion [21], and amines [22]. However, most of these solvents are toxic and difficult to separate from the volatile organic compounds for the recycling process [23]. The green absorbent materials should be

characterized by low vapor pressure, high boiling point, low viscosity, high absorption capacity, low cost and should be easy to regenerate [24].

Until recently, ionic liquids have been considered the ideal absorbents for the capture of BTEX from gaseous fuel streams [23]. However, their high price, non-biodegradable, and frequently toxic properties make them not widely used in the industrial purification of gaseous streams. In order to overcome the disadvantages of ionic liquids, a new type of green solvents named deep eutectic solvents (DESs) started to be considered as efficient media for biogas purification. According to the definition, DES is a complex which is consisting of a hydrogen bond donor (HBD) and hydrogen bond acceptor (HBA) with appropriate molar ratios. The specific non-covalent interactions created between HBA and HBD lead to the formation of DES with a much lower melting point compared to the individual components [25,26]. So far, many new DESs have been synthesized and successfully used in many separation processes, such as extraction, microextraction, absorption, and adsorption [27–32]. Literature data show that DES is characterized by a high absorption capacity of carbon dioxide and other inorganic pollutants (including ammonia, hydrogen sulfide, water vapor, and sulfur dioxide) occurring in gaseous fuels, i.e. biogas. However, to ensure high efficiency of the removal of individual contaminants, it is necessary to choose the appropriate substances for DES formation. This is a crucial parameter because, as proven in previous works, the driving force of absorption processes using DES are non-covalent interactions between the absorbent and impurities, i.e., hydrogen bonds or electrostatic interactions. For example, to absorb CO_2 (hydrogen bond acceptor), it is necessary to use a DES that has at least one hydrogen bond donor group in the structure, i.e. -OH, -COOH, or -NH_2. The opposite is true for ammonia, which, due to its structure, is a good hydrogen bond donor, therefore a suitable DES for absorption should have acceptor groups, i.e. =O, or -O- [33–38]. The mechanisms for removing inorganic contaminants from gas are currently fairly well known. Therefore, it is easy to speculate

which DES might be suitable for capturing selected substances. However, knowledge of the VOC absorption capacity of gaseous streams with DES is very limited. Until now, the high absorption capacity of deep eutectic solvents has been proven for volatile organic silicon [24,32,39,40], sulfur [41], and chlorine compounds [42]. Among the compounds from the BTEX group, an attempt has been made to remove toluene from biogas [43,44]. To the best of our knowledge, there are no works dedicated to the removal of all BTEX compounds from gas streams by means of deep eutectic solvents.

The paper describes the synthesis of new green monoterpenes based on deep eutectic solvents, their structural, and physicochemical properties (i.e. density, viscosity, surface tension, and melting point) as well as the application as efficient absorbents for BTEX capture from biogas. In this study, structural characterization of new absorbent materials and interaction between BTEX, and DES were analyzed using theoretical method based on the COSMO-RS model, and experimental techniques based on proton and carbon-13 nuclear magnetic resonance (^{1}H NMR and ^{13}C NMR), as well as Fourier transform infrared spectroscopy (FTIR). The absorption process was optimized in terms of the selection of the appropriate DES, and absorption temperature. Under optimal conditions, the absorption efficiency of DES was compared with a commercially available absorbent dedicated to biogas purification. The absorption processes were monitored using two methods, gas chromatography, and sensor matrices. The comparison of the two methods of process control was aimed at confirming the usefulness of the sensors' matrices in online research, due to shorter time of single analysis and its lower costs. The use of sensor arrays allow a real-time control of the absorption process, which in combination with an appropriately selected control algorithm can make the process fully autonomous (requiring little control by personnel). The validity of using gas sensor matrices as an alternative to chromatographic techniques has already been demonstrated, e.g. to control biofiltration process [45–48], odour monitoring

[49], methane reforming process monitoring [50] and they also have high application potential in food industry [51] or pharmaceutical industry [52].

2. MATERIALS AND METHODS

2.1.Materials

The following substances were used for the preparation of DES: ±camphor (Cam), carvone (C-one), eucalyptol (Eu), furfural (Fu), choline chloride (ChCl), tetramethylammonium bromide (TMABr), tetraethylammonium bromide (TEABr), tetrapropylammonium bromide (TPABr), tetrabutylammonium bromide (TBABr), guaiacol (G), syringol (S), menthol (M), thymol (Th), vanillin (V), formic acid (FA), octanoic acid (OA), nonanoic acid (NA), decanoic acid (DA), dodecanoic acid (DDA) and levulinic acid (Lev). For the preparation of contaminated biogas, monoaromatic hydrocarbons including benzene, toluene, ethylbenzene, and xylene were used. All reagents were obtained from Sigma Aldrich (St. Louis, MO, USA) with high purity (≥ 98%). For the comparison of DES efficiency, a commercially available absorbent Genosorb ® 1843 (Clariant, USA) was used. High purity gases including nitrogen (purity N 5.0), methane (purity N 5.5), and carbon dioxide (purity N 4.5) were obtained from Linde Gas (Poland). The air was generated by a DK50 compressor with a membrane dryer (Ekkom, Poland), and hydrogen (purity N 5.5) generated by Precision Hydrogen 1200 Generator (PEAK Scientific, Scotland, UK). All gases were used for the preparation of a model biogas streams and chromatographic analysis.

2.2.Procedures

2.2.1. Preparation of DESs

DESs were prepared using the method described in previous studies [40–42]. Two chemical compounds were mixed with each other in a proper molar ratio. In the next step, the

mixture was stirred on a magnetic stirrer at 60°C until a homogeneous liquid was formed. DES was cooled to the room temperature (RT).

2.2.2. Preselection of DESs based on Henry's law constant

The preselection of DES were prepared based on Henry's constants. Studies were performed using the headspace technique combined with gas chromatography-flame ionization detector (HS-GC-FID) in accordance with the procedure described in the previous works [53]. Only DES that were liquids at room temperature were used for the test. Liquid DES (0.5 mL) was transferred to 20-mL headspace vials to which the 0.75 μL of each BTEX compound was added. The vials were then sealed and incubated at room temperature for 24 hours. Then 100 μL of the headspace was introduced into the gas chromatograph. The concentration of BTEX in the gas phase (headspace) was determined on the basis of calibration curves prepared in accordance with the procedure presented in the previous works. The concentration of selected BTEX compounds in a liquid phase (DES) after headspace procedure was calculated according to Eq. 1:

$$V_1 \cdot C_0 = V_1 \cdot C_1 + V_g \cdot C_g \quad (1)$$

where: V_1 – DES volume [cm^3];

V_g – gas volume (headspace volume) [cm^3];

C_0 – initial concentration of BTEX in liquid sample (DES) [mol/m^3];

C_1 – concentration of selected BTEX in DES phase after headspace procedure [mol/m^3];

C_g – concentration of selected BTEX in gas phase after headspace procedure [mol/m^3];

The dimensionless Henry's law solubility constant was calculated according to Eq. 2:

$$H = \frac{C_g}{C_1} \quad (2)$$

2.2.3. Characterization of DESs

DESs viscosity and density measurements were made in the temperature range from 20 to 50 °C. Measurements were made using the following apparatus BROOKFIELD LVDV-II+viscometer (Labo-Plus, Poland), and a DMA 4500 M density meter (Anton Paar, Poland). The surface tension (ST) of DES was measured using a tensiometer (A KRŰSS K9 model K9MK1) in the range of temperature of 20-50°C. The tensiometer was stabilized for 30 minutes and calibrated using water at 20°C. Then the 4 mL of DES was placed in a thermostated measuring cup. After reaching the appropriate temperature, the ST of DESs was measured automatically using A KRŰSS K9 within 3 seconds. The melting point (MP) of DESs was determined visually by cooling eutectic mixtures to -25°C in a cryostat (HUBER, Germany). Then the temperature was increased at 1°C/min. The temperature at which the appearance of the first liquid drop was observed was taken as MP. Measurements of all physical properties of DES were repeated three times.

2.2.4. Mechanism of DESs formation, and BTEX absorption

The absorption mechanism and structural properties of new DESs were analyzed by ATR-FTIR spectroscopy by means of a Bruker Tensor 27 spectrometer (Bruker, USA) with an ATR accessory and OPUS software (Bruker, USA). The following parameters were adopted for the studies: 4000–600 cm^{-1}; the number of background and samples scans: 256; resolution: 4.5 cm^{-1}; slit width 0.5 cm. Additionally, nuclear magnetic resonance spectroscopy (NMR) measurements were performed in order to receive more deep insight into DES formation and the efficiency of BTEX absorption. Samples for NMR analysis were

prepared in 5 mm tubes by weighing 20 mg of DES and inserting 0.4 mL of chloroform-d1. The NMR analysis was done out at 20°C by means of Bruker Avance III HD 400 MHz (Bruker, USA).

For the theoretical examination of the mechanism of BTEX absorption, Conductor-like Screening Model for Real Solvents model (COSMO-RS) was used. For these propose, ADF COSMO-RS software (SCM, Netherlands) was used according to previous studies [40,42,54]. In the first stage, the geometry optimization of DES which were selected during HS-GC-FID analysis including Cam:OA, Cam:DA, C-one:OA, C-one:NA, C-one:DA, C-one:Lev, Eu:OA, main components of commercially available absorbent (i.e. tetraoxaoctadecane and pentaoxaheneicosane) and BTEX was prepared. The geometry optimization of all eight absorbent complexes in 1:1 molar ratio, and BTEX compounds was performed using the continuum solvation COSMO model at the BVP86/TZVP theoretical level. In order to find the most stable conformers of studied compounds, optimization studies were performed in the gas phase. In the next step, the vibrational analysis was performed to find conformers that corresponds to the true energy minimum. The full geometry optimization of studies compounds was prepared only for the most energetically favorable conformers. For all absorbents, the affinity to BTEX was calculated by means of activity coefficient according to Eq. (3).

$$\ln(\gamma_i) = \frac{u_i^a - u_i^p}{RT} \quad (3)$$

where: u_i^a – chemical potential of selected BTEX in absorbent;

u_i^p - chemical potential of pure BTEX compounds;

R - universal gas constant (8.314 J/mol);

T - temperature (K).

In order to visualize the charge distribution of absorbents and BTEX, the σ-profiles were calculated using the 3D surface charge densities.

2.2.5. Absorption and desorption process of BTEX

In this work, the absorption/desorption set-up was described in the previous work was used [42]. In the first stage, pure nitrogen was passed through a vial containing 1mL of each BTEX compound. The obtained contaminated gas via bubbling phenomena was diluted with a model biogas stream (CH_4: CO_2: N_2 in 5:3:2 volume ratio) to 2000 mg/m^3 concentration of BTEX. In the next step, the biogas stream was directed into the absorption column with an appropriate absorbent. The desorption process was carried out using the pure nitrogen barbotage method at elevated temperatures in the range of 100-120°C consistent with previous research [55].

During the absorption/desorption processes, the biogas samples were collected before and after introduction into the absorption/desorption column. The biogas samples were analyzed by gas chromatography and sensors matrix. Biogas purification processes were carried out until the concentration of BTEX in the inlet and outlet biogas were equal. In order to ensure the correctness of the results, the absorption processes were repeated three times. The absorption capacity (Q) was determined according to the previous studies [42]. To determine the absorption capacity of the absorbent, the volumetric flow rates of individual components of the gas mixture have been designated as the product of the volumetric flow rate of the gas mixture and the concentration of its components. For this purpose, by means of an Agilent ADM Flow Meter, the gas flow at the outlet of the absorption columns needs to be measured. Values of Q were calculated using Eq. (4-6):

$$\frac{d(m_{BTEX})}{dt} = (F_{IN} \cdot C_{IN}(t) - F_{OUT}(t) \cdot C_{OUT}(t)) \cdot \bar{\rho}_{BTEX} \quad (4)$$

$$m_{BTEX} = \int_0^{t_{sat}} [F_{IN} \cdot C_{IN}(t) - F_{OUT}(t) \cdot C_{OUT}(t)] dt \cdot \bar{\rho}_{BTEX} \quad (5)$$

$$Q = \frac{m_{BTEX}}{m_A} \quad (6)$$

where: m_{BTEX} – BTEX mass absorbed [g];

m_A- mass of absorbents used to obtain complete saturation [g];

t_{sat} – saturation time of absorbents [s];

C_{IN} – BTEX initial concentration in biogas [ppm v/v];

C_{OUT} – BTEX outlet concentration in biogas [ppm v/v];

$F_{IN,OUT}$ – Flow rate of the biogas at the inlet and outlet of the absorption column [m^3/s];

$\bar{\rho}_{BTEX}$ - average BTEX density at a given temperature [kg/m^3]

The absorptivity of BTEX was calculated using the following Eq. 7:

$$A = \frac{A_{IN} - A_{OUT}}{A_{IN}} \quad (7)$$

where: A_{IN} – initial total peak area of BTEX compounds;

A_{OUT} - total peak area of BTEX compounds after absorption process.

2.2.6. Process control

2.2.6.1. Chromatographic analysis

For the control of absorption/desorption process efficiency, biogas samples were analyzed by gas chromatography technique. In order to determine Henry's constants in static process and concentration BTEX in gas streams in a dynamic process, gas chromatograph Autosystem XL (PerkinElmer, USA) equipped with a capillary column an HP-5 (30 m × 0.25

mm × 0.25 μm) (Agilent Technologies, USA), and a flame ionization detector (GC-FID) (PerkinElmer, USA) was used. The chromatographic analysis was conducted under certain conditions: temperature of the oven 60°C, injection port temperature 250 °C; the injection mode split 5:1, detector temperature 300°C, the carrier gas – nitrogen (flow rate: 1 mL/min), amount of sample injected: 0.5 mL. For the determination of CH_4, CO_2, and N_2 in the biogas stream during the absorption process, the gas chromatograph GC MG#5 (SRI Instruments, USA) coupled to a thermal conductivity detector (GC-TCD), and equipped with a packed column Porapack Q (80/100, 2 mm ID) (Restek, USA) was used. The following conditions were used: temperature of the oven 40°C, injection port temperature 60°C, detector temperature 80°C, the carrier gas – helium (flow rate: 5 mL/min), amount of sample injected: 2.0 mL.

2.2.6.2.Chemical gas sensor

In order to continuously monitor and control the absorption treatment of biogas, a matrix consisting of the commercially available gas sensor was constructed. Basic information about gas sensors used is shown in Table S1. The gas sensors were housed in separate PTFE chambers. This approach makes it possible to prevent the emissions of organic compounds into the measuring chamber and further reduces the absorption and chemical transformations of the gaseous substances. Due to the dependence of the output signal from PID-A12 gas sensors on variations in temperature, humidity, and atmospheric pressure, a sensor that controls these parameters was placed in an additional chamber. As a result, the lack of linearity of the PID output signal observed at higher concentrations can be corrected in the software during data analysis. Whereas, NDIR sensors capable of monitoring the presence of carbon dioxide and methane in process samples provide an analog voltage output proportional to the concentration of these gases, which is simultaneously linearized and temperature compensated. The constructed matrix allowed control of total BTEX concentrations in the

range of 0 to 6600 mg/m^3 while carbon dioxide and methane concentrations were monitored in the range of 0-100% by volume. The gas flow at the outlet of the absorption column was measured using an Agilent ADM Flow Meter, which provides continuous, real-time measurement of volumetric flow rate.

2.2.6.3.Gas sensor array measurement

The gas sensor array experimental setup is presented in Figure S1. Process samples were collected at the inlet and outlet of the process and the bags made of TEDLAR film were used for this purpose. The three-way valve (V1) made it possible to alternate between the analyzed sample and the atmospheric air passing through the air filter to the measuring chamber. Purified air was directed to the measurement chamber after each analysis in order to regenerate the gas sensors and restore their input parameters. The flow rate of the sample and air was controlled using the rotation speed of the diaphragm pump. The pulse width modulation module (PWM) was responsible for regulating the supply voltage delivered to the pump motor, which fluctuations directly affect the pump speed and thus the flow rate. The sensor measurement was performed in the stop-flow mode: the sample flow time through the sensor chamber was 30 seconds, than by closing the valve (V2) the sample was retained in the chamber for another 30 seconds. Sensors signals were recorded using an analog-to-digital converter and processed by means of dedicated software. All manufacturer's requirements were taken into account when the electrical circuits for each sensor were prepared. The created system was controlled automatically by the Arduino control module. All analyzed samples were also subjected to gas chromatographic analysis, which was treated as a reference method.

2.2.6.4.Data analysis and processing

Data analysis and other calculations were performed using RStudio Desktop (v. 1.4.1717) software. Multiple linear regression (MLR) was selected as the calibration and validation model for the gas sensor array. Thus, linear relationships between independent (sensor's signals), and dependent (e.g. gas concentration, chromatographic peak area) variables were determined for carbon dioxide, methane, and total BTEX. Also, other methods of data analysis, e.g. Principal Component Analysis (PCA), Principal Component Regression (PCR), Partial Least Squares Regression (PLSR) can be used effectively for this purpose, especially when dealing with very complex sample matrices.

3. RESULTS AND DISCUSSION

3.1.DESs preparation and preselection

In the studies, all DESs were prepared by mixing HBA, i.e., Cam, C-one, Eu, Fu, ChCl, TMABr, TEABr, TPABr and TBABr, with different HBDs i.e. Lev, OA, NA, DA, DDA, G, S, V, M, Th and FA in 1:1 molar ratio. From 99 tested DES, only 39 eutectic complexes turned out to be liquids at room temperature. DES which met the first basic criterion of absorbents - were liquids at RT, were selected for further research. Due to the relatively large number of new DESs, a pre-selection of DES was performed. DES screening was performed based on the determination of Henry's constants. This parameter reflects the dissolving ability of BTEX in DES [56]. The obtained results are shown in Figure 1. The lower values of the Henry constants (H) correspond to the greater BTEX solubility in DES. The results indicate that the lowest values of H were obtained for xylene and ethylbenzene . Slightly higher values were obtained for ethylbenzene and the highest for benzene. This indicates that the alkyl groups form stronger non-covalent bonds with DES compared to the π interactions which is in line with previous work [57]. It can be observed that BTEX compounds have the greatest affinity to non-ionic deep eutectic solvents. The affinity of monoaromatic hydrocarbons to the

ionic ones is significantly lower. These phenomena can be explained by the occurrence of very strong interaction between the cation and the anion in DES structures, that are stronger than the bonds formed between the DES and nonpolar impurities [58]. The obtained results suggests that ionic interactions do not play a significant role in the BTEX absorption process. The most favorable results were obtained for DES consist of the monoterpenes acting as HBA in combination with carboxylic acids. The lowest Henry's constant values were obtained for DES consist of carvone, camphor, and eucalyptol as HBA, and carboxylic acids as HBD including: C:OA (1:1), C:DA (1:1), C-one:OA, C-one:NA, C-one:DA, C-one:Lev, and Eu:OA in 1:1 molar ratio. This suggests that the carboxyl group (-COOH) not only binds efficiently to the carbonyl group of the monoterpenes (= O) to form strong hydrogen bonds, but is also involved in the formation of strong interactions with BTEX compounds. Additionally, the specific structure of monoterpenes can lead to the formation of additional π-π interactions with monocarboxylic hydrocarbons. The coexistence of both types of interactions may affect the high absorption capacity of the new DES. Only DES with the highest absorption potential was used for further research.

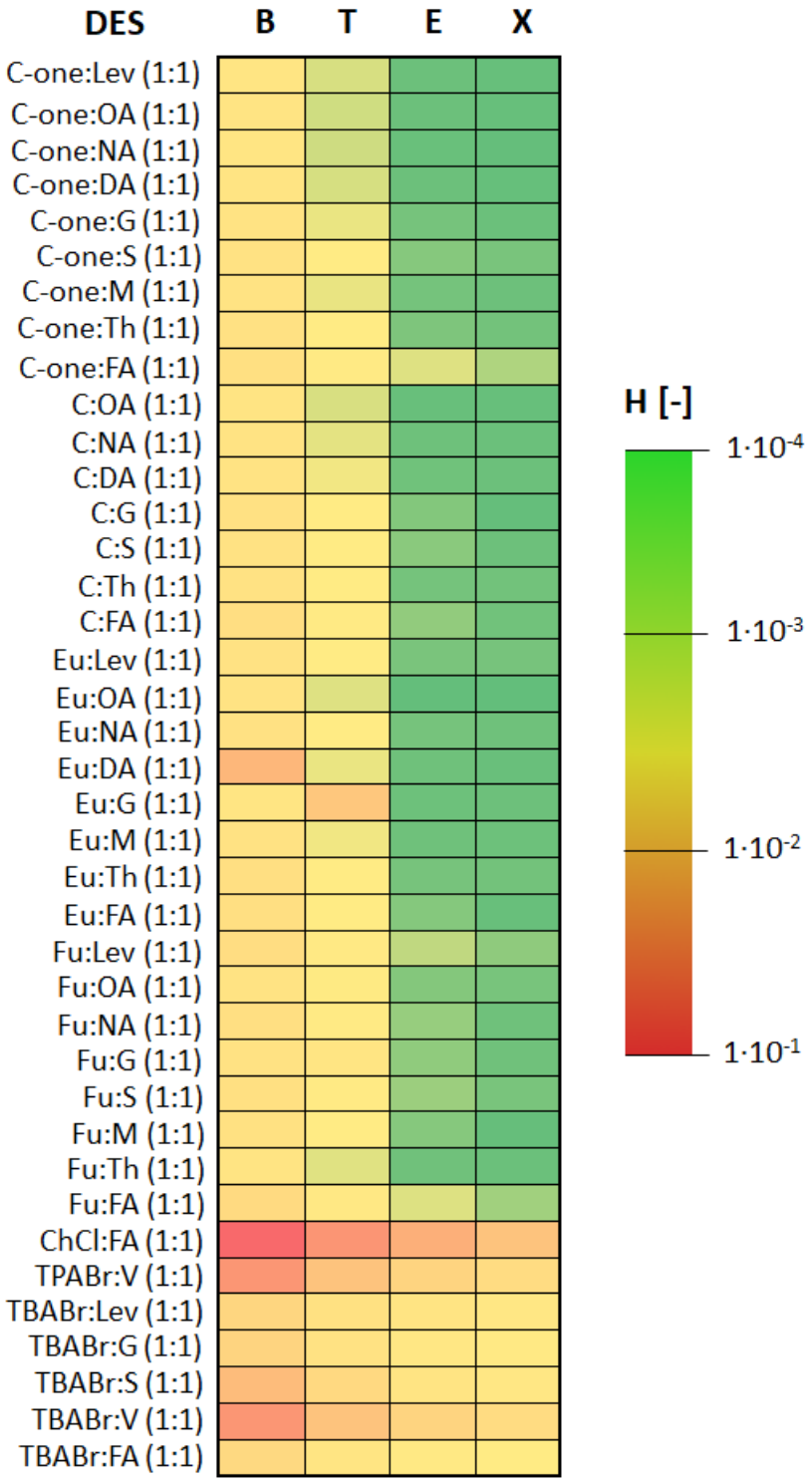

Figure 1 Henry's constants calculated for DES using the COSMO-RS model (according to the Eq. 2).

3.2.Mechanism of DES formation

Due to the synthesis of new DES, which have not been published so far, their detailed structural studies were performed. In addition, understanding the interaction mechanisms between HBA and HBD may play a key role in the selection of optimal absorbents for biogas purification. Therefore, in this study, FT-IR analysis were performed for new DES and their individual components. Figure S2 shows the FT-IR spectrum for the Eu:OA (1:1). On the DES spectrum, it can be observed the shift of wide bandwidth of stretching vibrations from O-H groups towards higher wavelengths (from 3002 cm^{-1} to 3014 cm^{-1}), and decreased peak intensity compared with the pure HBD. In the DES spectrum, intensity decrease, and shifts towards higher wavelengths are also observed for C=O stretching vibrations (from 1706 cm^{-1} to 1711 cm^{-1}) and C-O-C stretching vibrations (from 1080 cm^{-1} to 1081 cm^{-1}). The obtained results indicate that hydrogen bonding is formed between the carbonyl group from Eu and the carboxylic group from OA. Due to the presence of active oxygen atoms (-O-, or = O) in all tested HBA and carboxyl groups in HBD structures, similar band shifts can be observed in the spectra of the remaining DES (Figure S3-S8). This suggests the formation of strong hydrogen bonds between HBA and HBD in all tested DES [40,59].

In addition, ^{1}H NMR and ^{13}C NMR spectra were performed to confirm the formation of hydrogen bonds between DES components and for the identification of potential synthesis by-products. NMR spectra of Eu:OA (1:1) are presented in Figure S9, and the main shifts of peaks are summarized in Table S2. In the ^{1}H NMR spectrum, all identified peaks correspond to protons belonging to Eu and OA. This suggests that no by-products are formed during the DES synthesis.

Additionally, characteristic shifts in the ^{1}H NMR and ^{13}C NMR spectra of DES in comparison to pure substances can be observed. In ^{1}H NMR spectrum, mainly shifts toward lower values can be observed. The only exceptions are the (H1) and (H5) protons with Eu for which shifts towards higher values (from 2.02 to 2.19 ppm) can be observed. OA-derived

protons are characterized by greater shift values than protons from Eu. The largest shift can be observed for the (H1) proton (from 11.60 ppm to 11.03 ppm). This is a proton from the O-H group of the carboxyl group. Such a large shift (by 57 ppm) proves the direct participation of this group in the formation of hydrogen bonds in DES. In the ^{13}C NMR spectrum, the shifts of values for most C atoms from both HBA and HBD towards lower values can be observed. Only for (C1) and (C2) from Eu, the shifts towards higher values can be observed. These shifts are affected by the direct bond with the oxygen atom in the Eu molecule, which actively participates in the formation of a hydrogen bond. The highest value of the shift can be observed for (C1) from the OA molecule (from 180.81 ppm to 178.70 ppm). This is because the C atom from the carboxyl group is involved in the formation of the hydrogen bond. NMR spectra were also performed for the remaining DES. For the rest of DES, similar behavior can be observed. Spectra and a list of shifts are presented in Figures S10-S15.

3.3. Physicochemical properties of DESs

The practical application of DES requires knowledge of basic physicochemical properties including density, viscosity, surface tension, and melting point (MP). Therefore, all listed properties have been investigated in this work.

All studied DES are characterized by relatively significant depressions in melting point compared to pure HBA and HBD. MP of pure HBAs including Cam, C-one, and Eu are 175°C, 25.2°C, and 1.5°C, respectively. While the MP of pure HBDs i.e. Lev, OA, NA, and DA, were 33°C, 16.5°C, 12.3°C, and 31.6°C, respectively. The greatest decrease in MP can be observed for C-one:Lev (1:1) which equal -25°C. Slightly lower decrease in MP can be observed for the rest of DES including Eu:OA, C-one:OA, C-one:NA, C-one:DA, Cam:DA, Cam:OA, which are -23, -22, -21, -19, -19, and -8°C, respectively.

The density of DES is a crucial parameter that significantly affects the mass transfer processes. The literature data indicate that most DESs are characterized by higher density than

414 that of water, in the range of 1.00-1.35 g/cm^3 at 20°C [34]. The densities of the tested DES are
415 within the range of 0.9228 - 1.0397g/cm^3 at 20°C. The density values of studied DES follows
416 the order: C-one:Lev (1:1) > C-one:OA (1:1) > Cam:OA (1:1) > C-one:NA (1:1) > Cam:DA
417 (1:1) > C-one:DA (1:1) > Eu:OA (1:1). It can be observed that the density of DES closely
418 depends on the alkyl chain length of the carboxylic acids. An increase in the length of the
419 carboxyl chain causes the increase in molar volume, which affects the decrease in the density
420 value [60]. In addition, the density of DES strongly depends on temperature. The increase in
421 temperature of eutectic mixtures affects the increase in the kinetic energy of the DES
422 components, which causes a DES density decrease [61,62]. The densities of all tested DES at
423 20 – 50 °C are shown in Figure 2a.
424

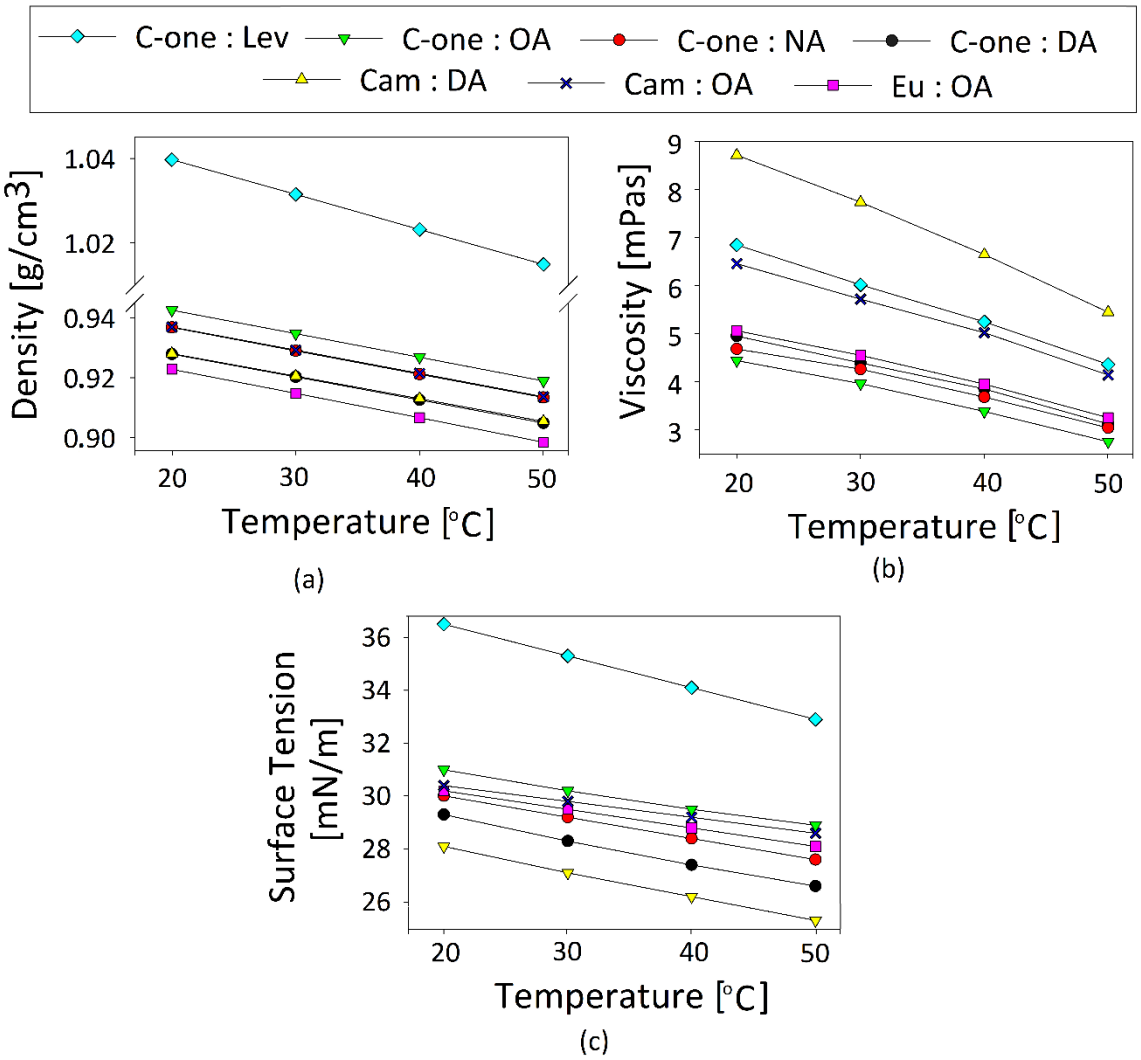

425

426 **Figure 2** The (a) density, (b) viscosity, and (c) surface tension (ST) of DESs in the
427 temperature range of 20-50°C.

428 The next important property of absorbents is dynamic viscosity due to their strong
429 influence on the mass transfer processes. Most DES are characterized by relatively high
430 viscosity (>100 cP) [25,26,63], which significantly limits their usefulness in absorption
431 processes. All tested DESs have lower viscosities than 10 mPas, and the value at 20°C
432 follows the order: Cam:DA (1:1) > C-one:Lev (1:1) > Cam:OA (1:1) > Eu:OA (1:1) > C-
433 one:DA (1:1) > C-one:NA (1:1) > C-one:OA (1:1). This indicates that all DES can be
434 successfully used for absorption. Obtained results indicate that the viscosity depends on the

structure of both HBA and HBD. It can be observed that the viscosity of DES increases with the increasing length of the alkyl chain. This is in line with previous studies [64]. The higher viscosity value of C-one:Lev (1:1) compared to C-one:OA (1:1), C-one:NA (1:1), C-one:DA (1:1) can be explained by the additional carbonyl group in Lev structure. In addition, Fan et al. proved that the lifetime of the hydrogen bond also influences the viscosity value, which decreases in DES systems where HBA belongs to monocyclic unsaturated terpene ketones [65]. The conducted research confirmed the theory of Fen et al. The lowest viscosity values were obtained for DES in which HBA was Carvone, which belongs to the group of terpene ketones. In addition, a close dependence of DES viscosity on temperature can be observed. As the temperature increase, the viscosity of DES decreases, which can be described by the Arrhenius or Vogel-Fulcher-Tammann model. This indicates the standard behavior of Newtonian liquids which can be explained by an increase in the average speed of DES molecules in the liquid phase at higher temperatures, which decreases the intermolecular forces. This causes a reduction of resistance of the fluid to flow and changes the viscosity [66]. Examined DES viscosity values at 20 – 50°C are presented in Figure 2b.

Another examined property of new DESs is surface tension (ST). This is another parameter that has a decisive effect on mass transfer process [67]. The surface tension of DESs strongly depends on many factors, such as the temperature, type, and nature (hydrophobic or hydrophilic) of HBA and HBD. Knowledge of ST provides important information about the molecular influence on the interactions in a mixture [68]. In this study, the ST of DES was measured in the temperature range of 20-50°C (Figure 2c). Typically ST of DES is in the range of 40 - 65 $mN \cdot m^{-1}$ at 25°C [69,70]. Experimental results indicate that the ST of studied DES composed of Carvone or Camphor as HBA and various carboxylic acids as HBD in a 1:1 molar ratio decreases with the increasing length of the HBD chain. This is probably due to the fact that with the increasing length of the acids chain the charge density

decrease thus decrease the importance of electrostatic interactions between HBA and HBD. In addition, the obtained results show that the ST of all DES decreases with the increase in temperature. This is in line with the typical behavior of the liquids [68]. As the temperature increases from 20°C to 50°C, a decrease in the ST value can be observed for C-one:Lev (1:1) from 36.5 mN/m to 32.9 mN/m, while for Cam:DA (1: 1) from 28.1 mN/m to 25.3 mN/m. This is due to the fact that increasing the DES temperature increases the molecular movement, the average kinetic energy, and reduces the forces of cohesion between molecules (weakening of the interaction between the HBA and HBD in DES) which causes the decrease in ST value [71,72].

3.4.Absorption of BTEX

One of the key factors which have a decisive effect on the absorption efficiency of BTEX is a type of DES. Therefore a DES pre-selection was performed. For this purpose, the absorption processes were carried out under optimal conditions obtained in previous studies [39,44]. The procedures for collecting data from sensors and gas chromatography are included in the S.1. - Supplementary Materials (Figure S16 - S17 and Table S3).

In the preselection studies, the only variable was the type of DES, and the other parameters were constant, i.e. temperature 25°C, biogas pressure 10 kPa, the volume of DES 50 mL, biogas flow rate 50 mL/min, and initial concentration of BTEX 2000 mg/m^3. The initial concentrations used were higher than the BTEX content in the biogas stream. However, the concentration was adjusted to the content of all aromatics compounds in the biogas, which is between 35 and 1731 mg/m^3 [74]. An inert gas - nitrogen was used as the gas matrix to exclude other interactions resulting from affinity to other biogas components. The experimental breakthrough curves of seven different DESs are presented in Figure 3. The obtained results indicate that the absorption capacity of BTEX depends both on the type of HBD, HBA, and the structure of BTEX. Based on a comparison of various DES composed of

485 octanoic acid as HBD and different HBA, it can be observed that the absorption efficiency is
486 ordered as follows, Eu > C-one > Cam. The time of effective absorption is 5852, 5556, and
487 4382 min for Eu:OA, C-one:OA, and Cam:OA, respectively. This order is due to the π-π
488 interaction between aromatic groups of HBA and BTEX. In addition, the C-one and Cam
489 contain in their structure the double bond of the carbonyl group that reduces structural
490 availability and reduces the hydrophobic nature of DES, which negatively affects the
491 effectiveness of the absorption process [75]. On the other hand, based on the comparison of
492 the efficiency of the absorption with the use of DES composed of carvone as HBA and
493 various carboxylic acids as HBD, the following sequence can be observed C-one:DA > C-
494 one:NA > C-one:OA > C-one:Lev. This is probably due to the fact that increasing the alkyl
495 chain length of the HBD affects decreases the polarities of DESs. The highly nonpolar nature
496 of DES has a positive effect on the rate and capacity absorption of BTEX [76]. The absorption
497 capacity is ordered according to the following sequence of BTEX: xylene > ethylbenzene >
498 toluene > benzene, which is consistent with a growing number of methylene groups in the
499 ring of impurities. The differences between breakthrough patterns can be explained by the
500 different interaction forces between BTEX and DES, as well as the physical properties of
501 selected absorbents. Benzene is mainly able to the formation of π interaction with the DES
502 functional group including –COOH, -CH_3, =CH_2, -O-, or =O. However, the strength of these
503 interactions is similar in each case [77]. Therefore, it can be assumed that the changes in the
504 breakthrough curves of benzene are caused by the physical properties of DES. A comparison
505 of benzene breakthrough curves shows a close dependence of DES supersaturation on their
506 viscosity. As viscosity increases, DES is supersaturated faster, which is due to the hindrance
507 of mass exchange. However, compounds that contain additional methyl or ethyl groups can
508 form both π and other weak hydrogen bond interactions with carbonyl, ester, or carboxylic
509 groups. As observed in previous studies, the strength of the weak hydrogen bonds (i.e. C-

H···O) interaction increases with the length of the alkyl chain in hydrocarbons. This indicates that the methyl groups are actively involved in the formation of non-covalent bonds with DES, which is in line with the results obtained from Henry's constants and with previous works [57,78]. However, differences in the saturation points of DES indicate that the basic physical properties, i.e. the dynamic viscosity of the absorbents, also can affect the absorption efficiency of T, E, and X.

DES composed of Eu and OA in a 1:1 molar ratio is characterized by the highest absorption capacity. This proves that not only the structure of DES components and the strongly hydrophobic nature of DES affects the efficiency of BTEX absorption, but also the physicochemical properties i.e. low viscosity, high surface tension, and relatively low melting point. Both types of parameters play a significant role in the absorption process and it is difficult to clarify which one is more important. However, the combination of favorable physical properties with the specific structure of Eu:OA enhances the effect of DES absorption capacity. Therefore, further research was only done for the most favorable DES.

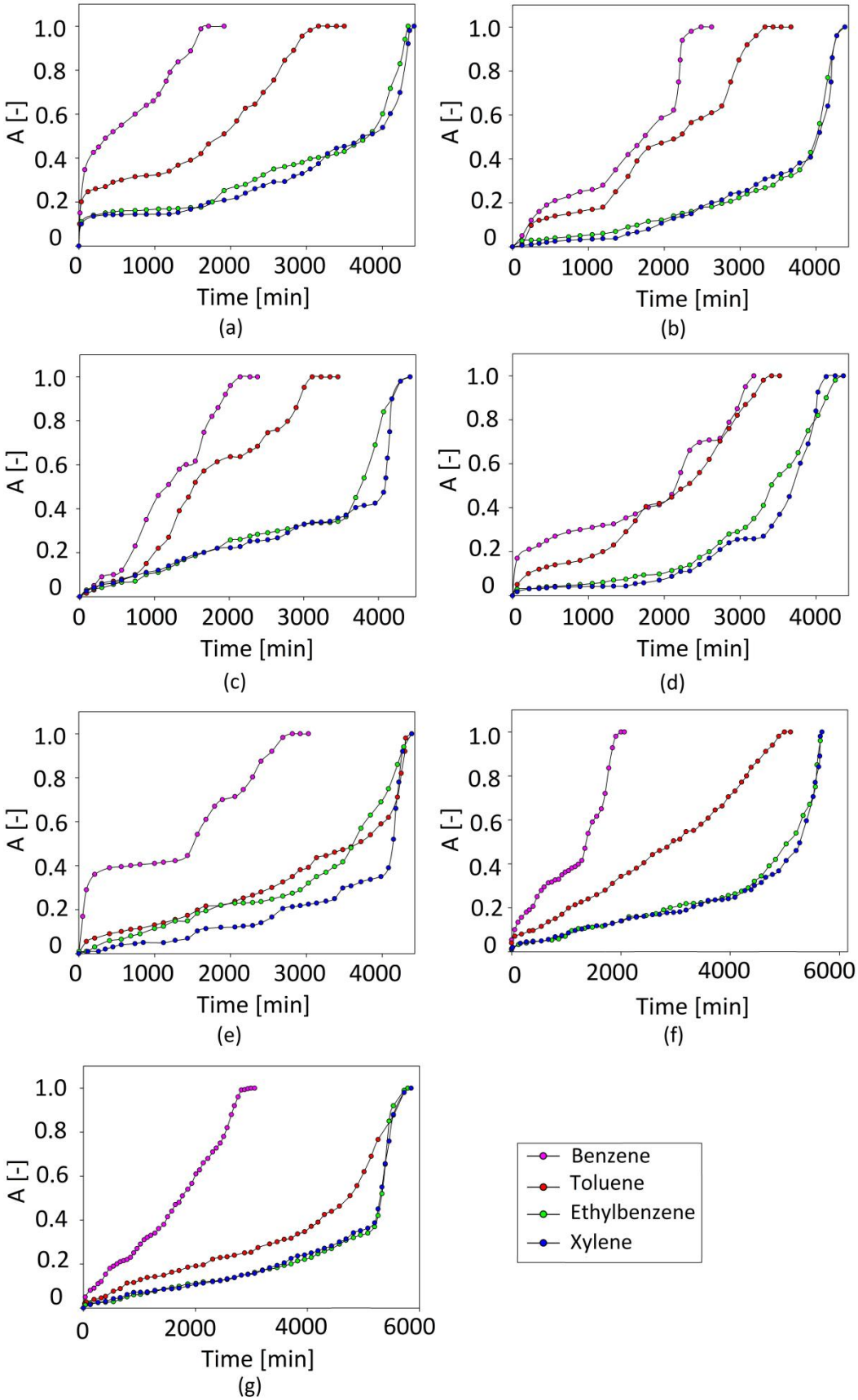

525

Figure 3 Experimental breakthrough curves of (a) Cam:DA (1:1); (b) Cam:OA (1:1); (c) C-one:Lev (1:1); (d) C-one:OA (1:1); (e) C-one:NA (1:1); (f) C-one:DA (1:1); (g) Eu:OA (1:1); on different DESs (temperature 25 °C; biogas (matrix gas N_2) flow 50 mL/min; inlet BTEX concentration 2000 mg/m^3); the volume of the DES 50 mL; absorption column dimensions: height 10 cm and width 3 cm.

As observed in previous work, the presence of other substances in the gas can significantly affect the absorption capacity of DES. Therefore, a quick comparison of Henry's constants (according to the Eq. 2) was performed for the absorption of single impurities and the entire BTEX mixture from biogas under static conditions. The outcomes are shown in Figure 4. The obtained results in the two variants are only slightly different from each other. This indicates that the coexistence of all BTEX in the biogas stream only slightly affects the absorption efficiency. This phenomenon can be explained by the lack of significant differences in the structures of all monoaromatic hydrocarbons, which could combine with functional DES groups and form competitive interactions.

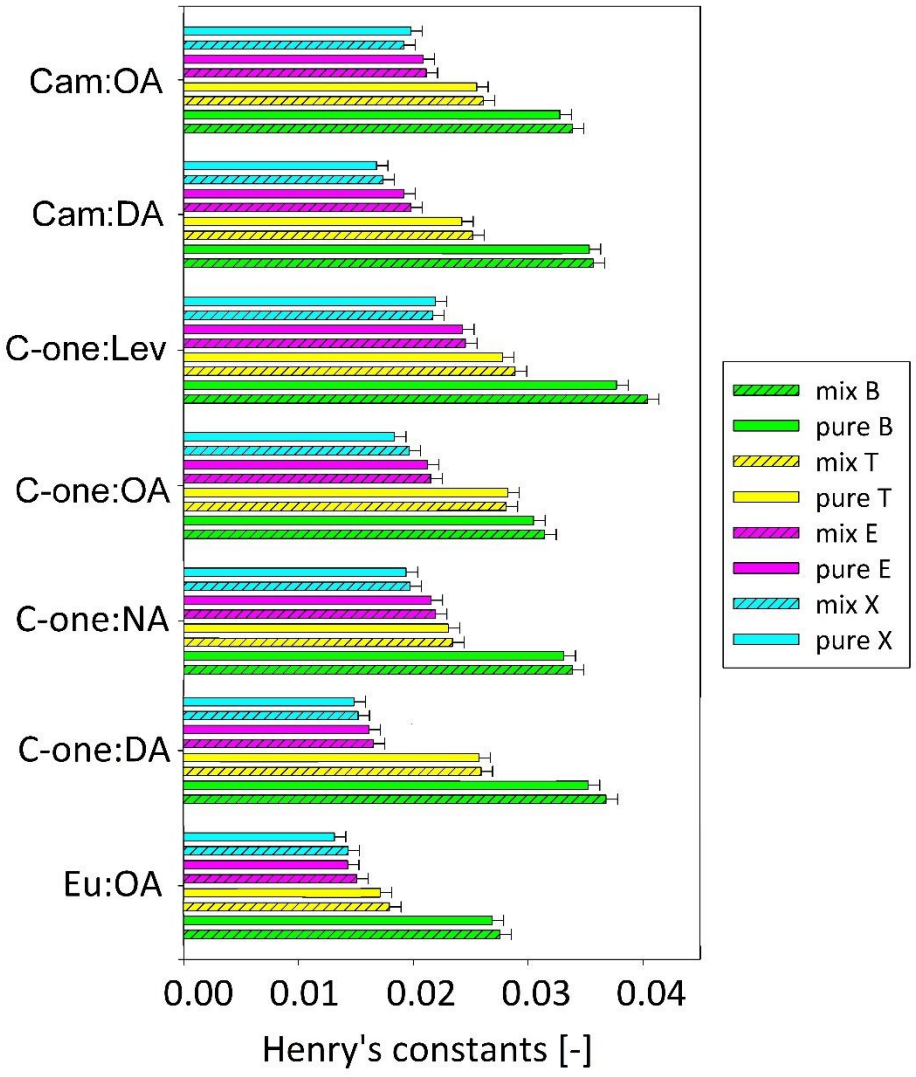

Figure 4 Henry's constants of the single impurities (solid column) and the BTEX mixture (hatch column) in DES. The total concentration of each of the impurities was 2000 mg/m^3, at 25ºC.

In the next part of the studies, the influence of the matrix effect on the DES absorption efficiency has been investigated (Figure 5). The BTEX absorption efficiency from pure nitrogen and from a model biogas mixture consisting of methane: carbon dioxide: nitrogen in a 5:3:2 volume ratio was compared. The composition of the model biogas mixture represents a typical matrix of real biogas streams [79]. The obtained results indicate that the type of gas matrix affects the effective time of BTEX absorption. It can be noticed that the use of a model

biogas stream reduces the absorption time and thus reduces the DES absorption capacity. This is due to the partial absorption of the main components of the biogas, i.e. CH_4 and CO_2. All tested DES are consist of HBA and HBD. Therefore, it is very likely that methane can easily bind to the hydrogen bond acceptor (CH_4···HBA), while carbon dioxide can easily bind to the hydrogen bond donor (CO_2···HBD), through non-covalent bonds [80]. Thus, competitive interactions can form that reduce the efficiency of BTEX uptake.

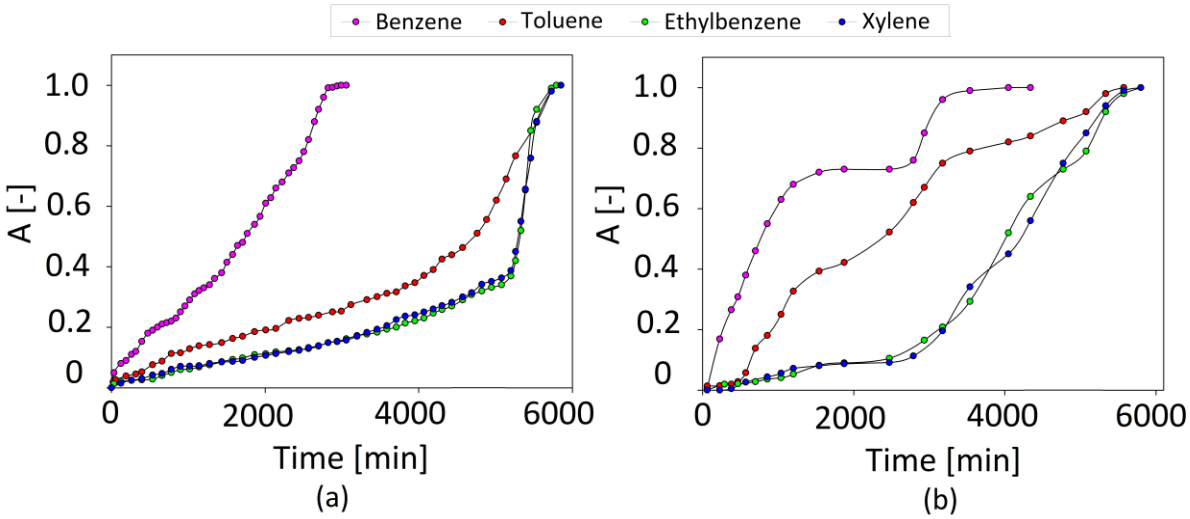

Figure 5 Experimental breakthrough curves of (a) Eu:OA (1:1) from pure nitrogen; (b) Eu:OA (1:1) from a model biogas mixture (CH_4:CO_2:N_2 5:3:2 volume ratios) flow 50 mL/min; temperature 25°C; inlet BTEX concentration 2000 mg/m^3, the volume of the DES 50 mL; absorption column dimensions: height 10 cm and width 3 cm.

In addition, the most favorable DES was compared with commercially available absorbent which is mostly consist of tetraoxaoctadecane and pentaoxaheneicosane. The obtained results are presented in Figure 6. The absorption processes were carried out using the model biogas mixture consisting of CH_4: CO_2: N_2 in a 5:3:2 volume ratio. The obtained results indicate that the new DES has an absorption capacity similar to that of a commercially available absorbent. The shortest impurities absorption time was obtained for the benzene, which was 4048

minutes. In turn, the longest time was obtained for the toluene, ethylbenzene, and xylene, which were 5334, 5790, 5800 minutes, respectively. The same BTEX removal trend can be observed for commercial absorbent. This indicates that the new DES may be a good alternative to commercially available sorbents. For which the shortest absorption time was achieved for benzene (3118 min). On the other hand, the absorption time was extended in the order of toluene, ethylbenzene and xylene, 4319, 5731 and 5859 min, respectively.

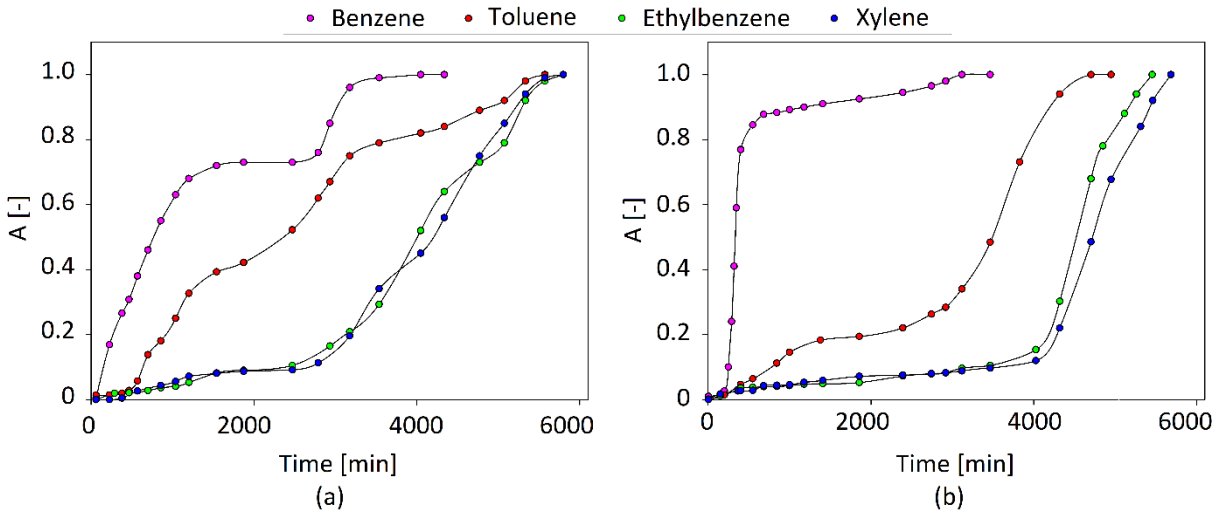

Figure 6 Experimental breakthrough curves of (a) Eu:OA (1:1) and (b) Genosorb (temperature 25°C; biogas (matrix gas: CH_4:CO_2:N_2 5:3:2 volume ratios) flow 50 mL/min; inlet BTEX concentration 2000 mg/m^3), the volume of the sorbent 50 mL; absorption column dimensions: height 10 cm and width 3 cm.

3.5.Mechanism of BTEX absorption

The absorption efficiency was also controlled at the structural level in order to explain the BTEX attachment mechanism for absorbents (DES and commercially available absorbent). For this purpose, the FT-IR and NMR analyses were carried out. Figure S18 show FT-IR spectra of the Eu:OA (1:1) and Genosorb before and after the absorption process. The mechanisms of BTEX absorption were also explained for the rest of tested DES. The results

585 are presented in Figures S19-S49. On the Eu:OA (1:1) spectrum after absorption process, the
586 characteristic peak from BTEX can be observed. The biggest changes are visible in the range
587 of 3123-3000 cm^{-1} (purple area), which can be assigned to the C_{Ar}-H stretching vibrations
588 occurring in the aromatic ring. In addition, the structural changes in DES after the BTEX
589 absorption process is also in the range 1631-1420 cm^{-1} (blue area), and 907-633cm^{-1} (pink
590 area). These changes are due to the emergence of the stretching vibrations C=C and the
591 deformation vibrations outside the plane C_{Ar}-H, respectively. The above described mentioned
592 chemical shifts suggest that the main driving force behind the BTEX absorption process is the
593 formation of hydrogen bonds between DES and the aromatic ring with BTEX. This fact is
594 also confirmed by the shifts signals with DES corresponding to the -OH groups from HBD
595 and C=O from HBA, which are shifted towards the lower wavenumbers, from 3431-3014 cm^{-1}
596 to 3415-3027 cm^{-1} and from 1711 cm^{-1} to 1708 cm^{-1}. For the remaining tested DES, very
597 similar shifts can be observed.

598 The similar results can be observed for commercially available absorbent. The
599 characteristic signals from BTEX are observed in very close ranges. In the spectrum after
600 absorption process the following signals can be observed C_{Ar}-H stretching vibrations in the
601 range of 3123-3000 cm^{-1} (purple area), stretching vibrations C=C 1631-1420 cm^{-1} (blue area),
602 deformation vibrations outside the plane C_{Ar}-H 907-633 cm^{-1} (pink area). The peak from the
603 C-O-C bond which are visible at the wavenumber of 1112 cm^{-1} on spectrum before absorption
604 is shifted towards higher values (Figure 7). This proves that ether group participates in the
605 attachment of BTEX to the absorbent. It can be concluded that there are absorbent-BTEX
606 bonds between the ether group (from Genosorb) and the aromatic group (from BTEX), which
607 are the driving force behind the BTEX absorption process.
608

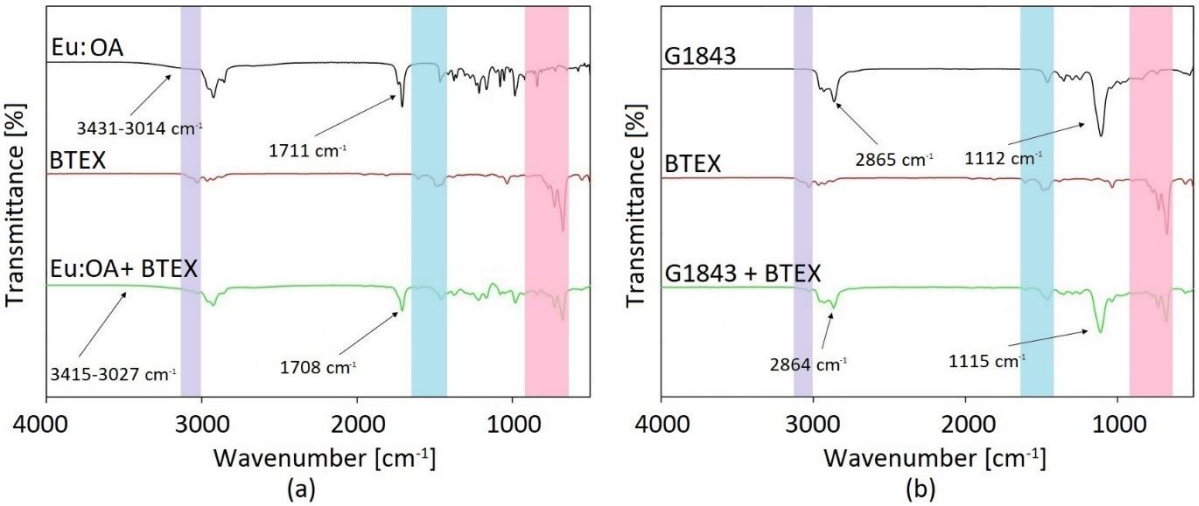

Figure 7 FT-IR spectrum before and after BTEX absorption for (a) Eu:OA (1:1) and (b) Genosorb.

In the ^{1}H NMR and ^{13}C NMR spectra of both Eu:OA (1:1) and Genosorb after the absorption process all visible peaks can be assigned to specific atoms derived from the Eu:OA (1:1) and BTEX (Figure S50). This confirms that the absorption process is a physical one, without the formation of other substances by the reaction. In the ^{1}H NMR and ^{13}C NMR spectrum for Eu:OA (1:1) after the absorption process can be observed the shifts towards the higher values. For HBD the biggest differences in the NMR spectrum can be observed for protons (H1) and the carbon atom (C1), which are derived from the carboxyl group the octanoic acid. The described differences are at the levels 0.48 ppm and 0.9 ppm. In the case of HBA, the biggest differences can be observed for protons (H6), which come from the methyl group in close contact with the O atom, and the carbon atom (C6) which forms a $-CH_3$ group connected to an aromatic ring. The described differences signals are at the levels of 0.34 ppm and 0.46 ppm. This indicate that the interactions between BTEX and DES are mainly caused by the van der Waals forces between the aromatic ring and the carboxyl group of HBD. Similar behavior can be observed for Genosorb. All peaks in NMR spectra are shifted towards the higher values. Detailed values of chemical shifts for Eu:OA and Genosorb are presented in Table S4.

In order to understand the electrostatic interactions between absorbents and BTEX, σ-profiles were calculated. According to the definition, σ-profiles is a distribution function that relates the surface area of a molecule to the charge density of the surface [81]. Based on profiles results, it is possible to predict how the BTEX molecules will interact in an absorbent solute system, as well as the selectivity and solubility of BTEX in absorbents. In these studies, the generated σ-profile diagrams were divided into three regions. The segment between -0.0082 e/Å^2 and +0.0082 e/Å^2 charge density show that the studied compound readily undergoes van der Waals interactions. Segments below -0.0082 e/Å^2 and above +0.0082 e/Å^2 indicate that the molecule represents the possibility of the formation of hydrogen bonding. For all studied DES and commercially available absorbents, peaks in all segments can be identified (Figure 8 and S51). However, the largest peaks are in the non-polar part and much smaller peaks are located in the HBA and HBD regions. The -O- and =O groups are responsible for the presence of peaks in the HBA region, and the -COOH group in the HBD region. This indicates that strong hydrogen bonds were formed in DESs between the HBA and HBD components. In order to confirm the obtained results, the electrostatic potential (ESP) analysis was also performed. The results are presented in Figure 11 and S47 which show the ESP mapped electron total density with an isovalue 0.001 au for absorbents, and BTEX. The red area shows the negative potential region (−40 kcal/mol), the blue part of the surface represents the positive potential area (40 kcal/mol), and the white part - is the non-polar region (0 kcal/mol). In DES molecules, electropositive areas are located around the H atom in –CH_3, -CH_2, -CH, and –COOH groups. The electronegative regions are located in –O-, and =O group from HBA, and neutral regions are located in both HBA and HBD molecules around carbon atoms. When DES is created, the electronegative area from HBA attracted the electropositive area from HBD. Thus, strong hydrogen bonds are formed between the DES components. The presence of large non-polar surfaces also indicates that additionally, weaker

non-covalent interactions, i.e. van der Waals interactions, are created between the DES components. Similar interaction can be observed between BTEX and DES or commercially available absorbent. Due to the presence of mainly non-polar regions in DES structures, weaker electrostatic interactions are the most likely driving force for the absorption process.

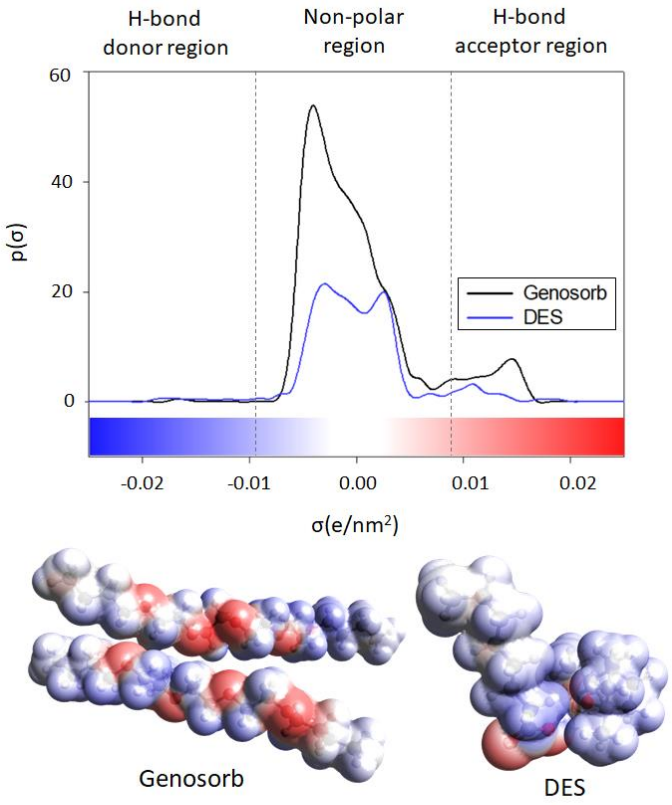

(a)

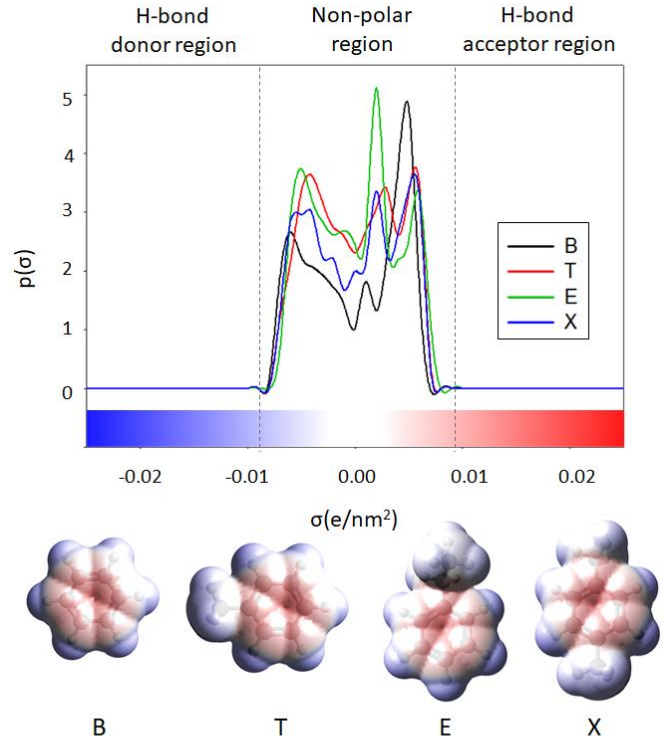

(b)

657

Figure 8 Sigma profile and electrostatic potential maps of a) Eu:OA (1:1) and commercially available absorbent; b) BTEX generated through COSMO-RS model.

3.6. Increasing the scale of the absorption process

For the most favorable DES, the absorption process was also performed on an enlarged scale in order to confirm the usefulness of DES. The scale-up included a 10-fold increase in the volume of absorbent to 500 mL and increasing gas flow rate up to 500 mL/min. The processes were carried out on a model biogas stream consist of CH_4:CO_2:N_2 in 5:3:2 volume ratios. The absorption process was made in two temperature variants. The first of the absorption column was maintained at room temperature (RT) and the second absorption column was cooled to 10°C. The absorption curves are presented in Figure 9. Based on the received data, similar absorption results can be observed compared to tests performed on a laboratory scale. In both processes, the order of saturation of the absorbent with aromatic compounds decreases with the decreasing volatility of the compounds. Benzene in both processes first breaks through the absorbent. The process of effective benzene capture is almost two times shorter compared to other substances. The DES breakthrough time for benzene is 5000 min and 6500 min in 25 and 10°C, respectively. The dependence of DES absorption capacity on temperature is also visible for other monoaromatic hydrocarbons. The duration of absorption at a temperature reduced is proportionally higher compared to room temperature, for toluene from 10500 min to 13700 min, for ethylbenzene and xylene from about 11500 min to 15000 min, respectively. The relationship between the increase in the efficiency of the absorption process and the decrease in temperature is well known and results from the exothermic nature of the absorption process [82]. Absorption curves for ethylbenzene and xylene have a similar shape and a similar breakthrough time, which is associated with a large chemical similarity of both compounds. In addition, it can be observed that the absorption rate for less volatile compounds increases when the more volatile

compounds (for example benzene) have already saturated the absorbent. This is probably due to the attachment of the remaining monoaromatic hydrocarbons to the already absorbed molecules through π-π interactions.

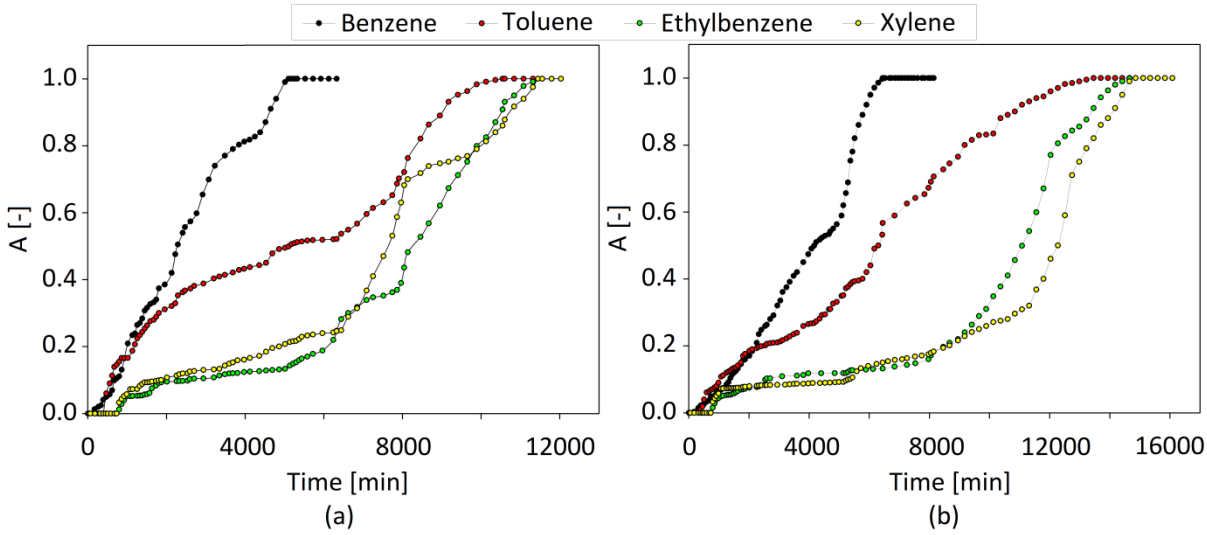

Figure 9 Absorption of BTEX (a) room temperature and (b) at 10°C; absorption column dimensions: height 30 cm and width 5.5 cm

By integrating the areas under the obtained curves over time, the total volume of methane, carbon dioxide, and BTEX used during the process was calculated (Figure 52). Then, assuming the density of substances, their masses were determined. The sorption capacity was calculated as the ratio of the difference between the determined masses of individual compounds in the inlet and outlet streams and the mass of the absorption liquid. Additionally, the degree of absorption of gas stream components during the process was determined. All the results obtained in this way are summarized in Table 1.

Table 1 Absorption capacity of DES.

Compound	Inlet stream		Outlet stream		Calculated parameters		
	V [m^3]	m [g]	V [m^3]	M [g]	Δm [g]	Capacity	Degree of

						[mg/g]	absorption [%]
Process in 10°C							
CO_2	1.3	2375	1.25	2356	18.6	40	0.78
CH_4	3.1	2132	3.1	2115	17.4	37.3	0.81
BTEX	0.011	45.3	0.0049	20.2	25.1	53.9	55.4
Process in 25°C							
CO_2	0.94	1765	0.93	1749.1	16	34.4	0.91
CH_4	2.44	1666	2.42	1654.2	12.2	26.2	0.73
BTEX	0.011	45	0.0052	21.5	23.2	49.7	51.9

The obtained results indicate that degree of BTEX absorption increase from 51.9 to 55.4% with decreasing temperature from 25 to 10°C. The same tendency can be observed for methane. For this molecule the degree of absorption increase from 0.73 to 0.81%. From the industrial absorption processes perspective, the increase in CH_4 solubility in absorbents is unfavorable, due to the fact that most industrial processes are carried out at 10°C. However, the increase in methane solubility is insignificant. The acceptable solubility of methane in the absorbent is 2% [83]. The opposite behavior can be observed for carbon dioxide. However, the solubility of CO_2 in DES is also negligible. Therefore, it can be concluded that the absorption process is selective for compounds from the group of monoaromatic hydrocarbons.

3.7.Comparison of process control methods

During the studies, two alternative methods for the control of absorption capacity were tested. Instrumental (analytical) techniques and a matrix of chemical gas sensors were used for process control and monitoring of tests performed. Gas chromatography with a flame

ionization detector (GC-FID) and thermal conductivity detector (GC-TCD) were used as a reference method, which allowed qualitative and quantitative analysis of chemical compounds present in the tested samples.

The commercially available gas sensors were selected to construct the array and based on the signals received the mathematical models were developed. They show the correlation between the results obtained using the reference technique and sensor matrix. The use of widely available sensors makes it possible to easily reproduce the constructed array and to duplicate it many times, which would be difficult to achieve in the case of testing prototype sensors.

The prepared sensors array was calibrated and validated using Multiple Linear Regression (MLR). Since the process was conducted at two different temperatures, which are 10°C and 25°C, it was decided to develop separate models for each of these cases. This approach allowed to determine the impact of the absorption liquid components on the obtained gas sensor signals. It was expected that the eucalyptol emission, which was a component of the absorption liquid used, would affect the signals from the gas sensors, particularly the PID sensor. For this reason, based on the recorded matrix response signals six MLR models were developed: for the inlet stream (total BTEX in 10°C and total BTEX in 25°C) and outlet stream (total BTEX in 10°C and total BTEX in 25°C), one common MLR model for carbon dioxide inlet and outlet streams and one for methane in the same configuration. The MLR models for BTEX were developed to return the predicted total area of the chromatographic peaks of these compounds. Correlation charts for inlet and outlet streams, showing the accuracy of the prepared models, are presented in Figure 10.

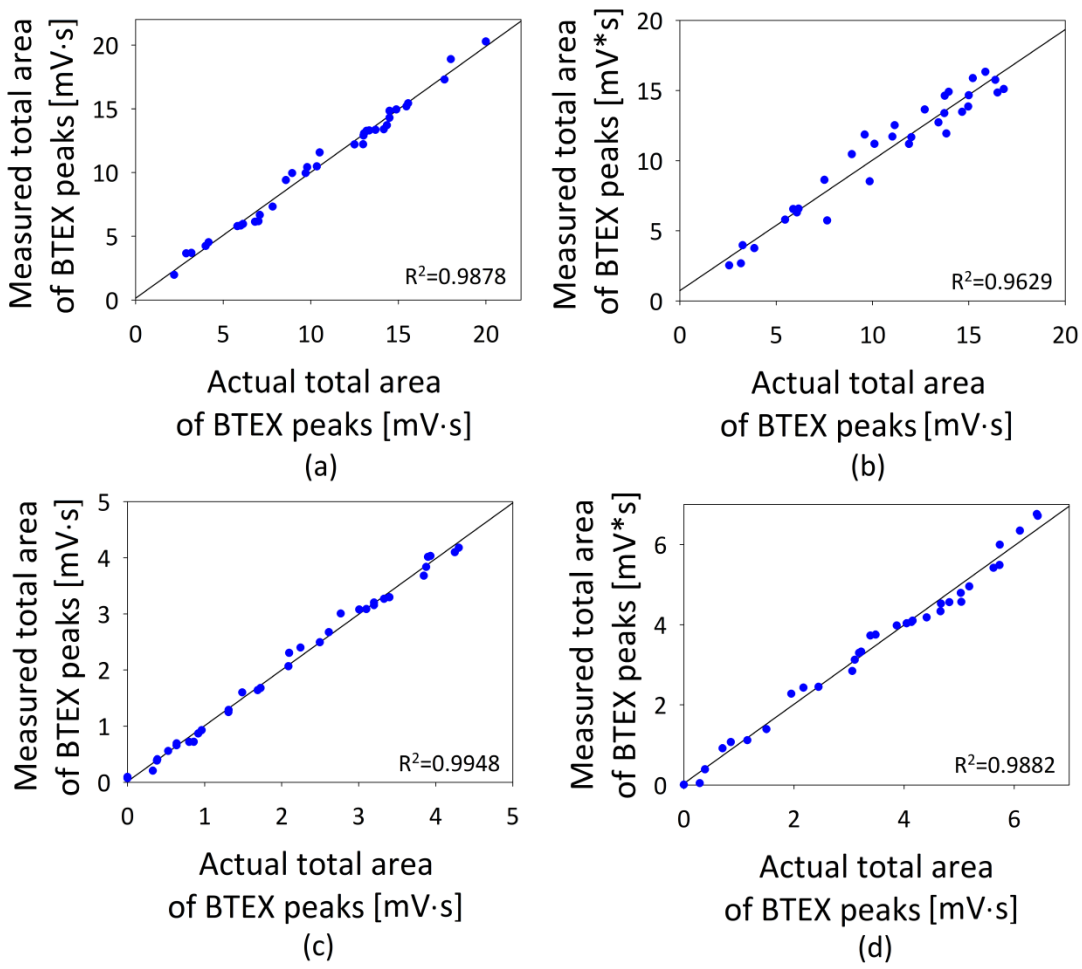

733

734 **Figure 10** Actual and determined total area of chromatographic peaks correlation plot for
735 inlet stream: (a) BTEX in 10°C, (b) BTEX in 25°C and outlet stream: (c) BTEX in 10°C, (d)
736 BTEX in 25°C

737 For methane and carbon dioxide, model gas mixtures were prepared to reflect the
738 expected concentrations of these gases at the inlet and outlet streams of the process. The
739 composition of the binary gas mixtures is shown in Table S5. The gas sensor array response
740 was recorded for each mixture, with the analysis repeated three times. The number of gas
741 calibration mixtures prepared was 42. Correlation charts of MLR models prepared for
742 methane and carbon dioxide are shown in Figure 15.

743 The validity of using this method is confirmed by the values of the coefficients of
744 determination (R^2) in the correlation plots. The value of coefficients of determination between

chromatographic results and the values returned by prepared models are shown in Table S5. For five of the six prepared models the values of R^2 were more than 0.9850. The lowest values of R^2 was achieved for the BTEX inlet stream at 25°C and was equal to 0.9629, which is still more than satisfactory. It should be noted that eucalyptol emission in outlet streams clearly affects the signals from the PID sensor. Additionally, the emission depends on the process temperature. This is shown by the intercept values in the outlet stream models. Only after reduction of the matrix response to this eucalyptol the BTEX concentrations calculated using the prepared MLR models are similar to those obtained by chromatographic methods.

The developed MLR models were used to calculate the quantitative parameter of the description of the absorption process, which was absorptivity. The results of sensor matrices were compared with gas chromatography, which was a reference method. Figure S53 presents the absorptivity parameter determination using a gas sensor array and gas chromatography throughout the process. The Root-Mean-Square Error (RMSE) for the entire range is presented in Table S6. RMSE is equal to 0.017 for the BTEX in the process carried out in the temperature of 10°C, and 0.067 for the BTEX absorption process in 25°C. In the case of methane and carbon dioxide the mean square errors reached slightly higher values. They were equal to 0.024 and 0.028 for methane in 10°C and 25°C . For carbon dioxide the calculated RMSE values are very similar as they are 0.031 at 10°C and 0.039 in 25°C respectively.

The obtained results indicate that the values of the total concentration of BTEX, CH_4 and CO_2 in biogas at the inlet and outlet do not differ significantly from this obtained using reference techniques. Additionally, such results demonstrate that sensor matrices could be satisfactorily used to control and monitor the absorption biogas purification processes. This study confirmed that the results obtained with the gas sensor array together with an appropriately selected mathematical model might be of similarly high level of quality as the results obtained using the gas chromatography technique (Figure 11).

One of the limitations of sensor matrices is the possibility of measuring only the sum of BTEX concentration. There is no possibility to receive separate signals for individual compounds (inability to conduct qualitative analysis). However, from an industrial point of view, there is no need to measure separate compounds. Much more important is to measure the sum of impurities. A few additional challenges during sensor measurements are: the influence of temperature and humidity on the stability of the sensor's signals, multidimensionality of the generated signals (requires averaging by statistical methods) or complicated calibration on the basis of analytical procedures and regression models. Moreover, it should be noted that the research was conducted at laboratory scale. For this reason, the constructed array would not be able to be used directly in the process stream, but the next step will be to adapt the sensor array for operation under real conditions, e.g. using a dilution module to reduce gas concentration to required ranges.

Chromatographic techniques are characterized by high repeatability, reproducibility and accuracy and they give the possibility to identify all compounds present in a tested sample. In this regard, sensor arrays are no match for the instrumental techniques but if it is important to reduce the time of the analysis, investment costs or to automate the measurement process, they are an excellent alternative. Ultimately, gas sensor matrixes are intended to bridge the gap between gas sensors that are selective for specific chemical compounds and chromatographic techniques, which have a much broader field of application but are unsuitable for real-time measurements and require periodic maintenance and ensure the availability of high purity gases.

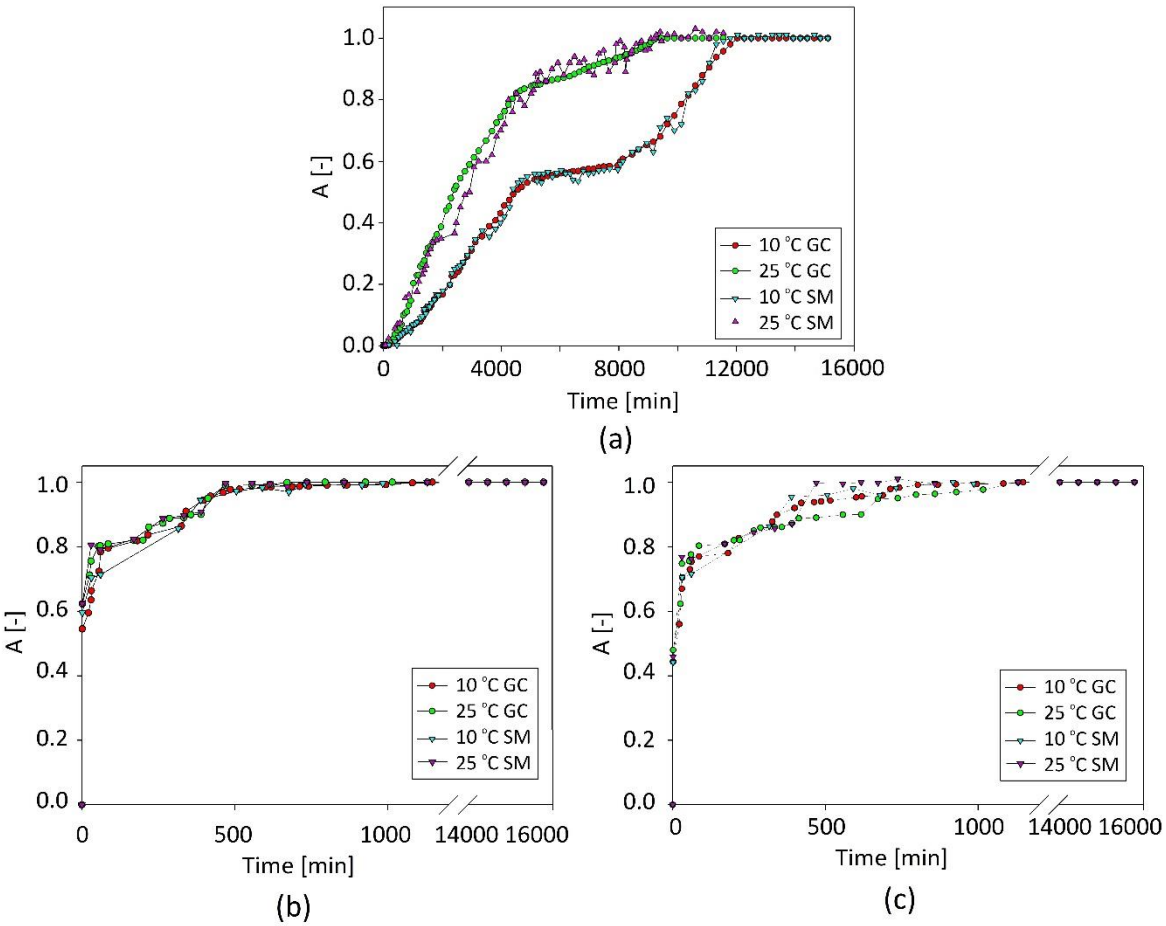

792

793 **Figure 11** Absorption of (a) sum of BTEX; (b) CH_4; and (c) CO_2 controlled by gas
794 chromatography (GC) and sensory matrix (SM).

795 **3.8.Regeneration process of DES**

796 From an economic and practical point of view, regeneration of the absorbents is a crucial
797 feature. Therefore, the DES regeneration processes after BTEX absorption were performed.
798 The desorption process was carried out using conventional nitrogen barbotage in the
799 temperature range 100-120°C method. Based on the obtained results, it can be observed that
800 with the increase of the desorption temperature, the time of total BTEX removal was
801 significantly shortened. At 120°C, complete BTEX desorption was obtained after 1 h. In order
802 to confirm the BTEX absorption-desorption capability, DES after regeneration was subjected

into another absorption process. As shown in Figure S54, hydrophobic Eu:OA (1:1) retains effective BTEX absorptivity at 95–97% during even ten consecutive regeneration cycles.

The absorption-desorption efficiency was also controlled at the structural level. Due to this the ^{1}H NMR, ^{13}C NMR and FT-IR absorption. The results are shown in Figure S55. In all spectra, the signals from the BTEX that were identified in Figure 18 have disappeared. The spectra of fresh and regenerated DES are almost identical, which indicates that DES does not change its structure during the desorption process.

3.9.Comparison of DES with other solvents

Currently, there are only a few studies in the literature relating to the absorption of BTEX from gas. Most of the work concerns the removal of toluene using ILs or DES. The comparison of DES efficiency with literature data is presented on Table 2. The obtained data indicate that Eu:OA (1:1) is characterized by higher absorption capacity of monoaromatic hydrocarbons in comparison to other DES, but the values are slightly lower than ILs. However, the cost of producing absorbents based on ILs is many times higher than for DES. In addition, the ILs have many others disadvantages such as the complicated synthesis, toxicity, and poor biodegradability. The disadvantages of ILs limit their large-scale use in absorption processes.

Table 2 Absorption capacity of toluene in various solvents.

Type of solvents	**Abbreviation**	**Absorption capacity [g/g]**	**Gas matrix**	**Temperature [^{o}C]**	**Price [€/kg]**	**Pressure [atm]**	**Literature**
DES	Eu:OA (1:1)	0.056	model biogas (CH_4 50%, CO_2 30%, N_2 20%)	10	43	1.0	This study

DES	Eu:OA (1:1)	0.050	model biogas (CH_4 50%, CO_2 30%, N_2 20%)	25	43	1.0	This study
DES	LauA:DecA (1:2)	0.0035	nitrogen	30	27	n.d.	[76]
DES	Lid:DecA (1:2)	0.0023	nitrogen	30	533	n.d.	
DES	Thy:DecA (1:2)	0.0021	nitrogen	20	41	n.d.	
DES	TBPB:DecA (1:2)	0.00080	nitrogen	30	183	n.d.	
DES	DecA:OctN (1:2)	0.00068	nitrogen	30	18	n.d.	
DES	ChCl:Res (1:2)	0.00051	nitrogen	30	71	n.d.	
IL	[Bmim][NTf_2]	0.22	air	20	1600	1.17	[84]
IL	[Dmim][NTf_2]	0.34	air	20	6263	1.17	
IL	[Emim][Ac]	0.51	n.d.	25	1180	1	[23]
IL	[Bmim][NTf_2]	0.15	n.d.	25	1600	1	
IL	[Bmim][Otf]	0.18	n.d.	25	1430	1	
IL	[Omim][PF_6]	0.31	n.d.	25	7920	1	
IL	[Hmpy][NTf_2]	0.21	n.d.	25	11860	1	
IL	[EMIM][BF_4]	0.12	synthetic air (21% O_2 and 79% N_2)	25	1330	1	[85]
IL	[BMIM][BF_4]	0.24	synthetic air (21% O_2 and 79% N_2)	25	929	1	
IL	[HMIM][BF_4]	0.38	synthetic air (21% O_2 and 79% N_2)	25	16800	1	
IL	[BMIM][I]	0.17	synthetic air (21% O_2 and 79% N_2)	25	5600	1	
IL	[BMIM][PF_6]	0.29	synthetic air (21% O_2 and	25	2276	1	

			79% N_2)				
IL	[BMIM][HSO_4]	0.070	synthetic air (21% O_2 and 79% N_2)	25	1250	1	
IL	[BMIM][CH_3COO]	0.40	synthetic air (21% O_2 and 79% N_2)	25	1380	1	

4. CONCLUSIONS

Deep eutectic solvents based on monoterpenes were successfully synthesized and applied for BTEX absorption from the biogas stream. The most important structural and physicochemical parameters that affected absorption efficiency were carefully studied. The obtained results indicate that DES consists of monoterpenes and carboxylic acids that are able to form strong hydrogen bonding and other weaker non-covalent interaction between active groups from HBA and HBA. The result of the interaction is the formation of stable eutectic mixtures, with a much lower melting point compared to pure ingredients, and favorable physicochemical properties, i.e. viscosity, density, and surface tension. From the tested DES, E:OA (1:1) is characterized by the highest absorption capacity of compounds from the BTEX group. This is due to the combination of its favorable physicochemical properties and the specific structure which selectively captures monoaromatic hydrocarbons by the formation van der Waals and π-π interactions between BTEX and DES. Absorption capacity depends on the absorption temperature and matrix composition. BTEX absorption capacity can vary from 0.05 to 0.056 g/g, which is comparable to commercially available absorbents. In addition, the low cost of DES production, the possibility of multiple regenerations without affecting the DES structure and without a significant reduction in the absorption efficiency, make DES an excellent green alternative to other absorption media.

Process control and monitoring was carried out using chromatographic techniques and self-constructed matrix of gas sensors. The controlled parameters of the absorption biogas treatment determined with the use of sensory techniques represents a similarly high level of quality as the results obtained with the gas chromatography. Thus, it was confirmed that real-time monitoring of absorption process is possible and there is no need to take any samples, conduct periodic maintenance of chromatographs and ensuring the availability of high purity gases. In other words, the analyzes showed that very similar or even identical results can be obtained faster and cheaper using gas sensors array, but they do not allow quantitative analysis of tested samples. We conclude that the prepared sensor array, with the use of slight technical improvements, could be used on an industrial scale to supervise and control the ongoing process in real time in order to automate the process analysis.

ACKNOWLEDGEMENTS

This work was supported by Gdańsk University of Technology under the Argentum Triggering Research Grants—EIRU program Grant (No. DEC-34/2020/IDUB/I.3.3).

NOTES

The authors declare no competing financial interest.

REFERENCES

[1] What is BTEX and why is it important?, (n.d.). https://www.aeroqual.com/blog/what-is-btex (accessed March 29, 2022).

[2] J.G.C. Bretón, R.M.C. Bretón, S.M. Morales, J.D.W. Kahl, C. Guarnaccia, R. del

Carmen Lara Severino, M.R. Marrón, E.R. Lara, M. de la Luz Espinosa Fuentes, M.P.U. Chi, G.L. Sánchez, Health risk assessment of the levels of BTEX in ambient air of one urban site located in leon, guanajuato, mexico during two climatic seasons, Atmosphere (Basel). 11 (2020). https://doi.org/10.3390/atmos11020165.

[3] K.A.U. Johansson, Characterisation of contaminants in biogas before and after upgrading to vehicle gas, Rapp. SGC 246. (2012).

[4] F. Abbasi, H. Pasalari, J.M. Delgado-Saborit, A. Rafiee, A. Abbasi, M. Hoseini, Characterization and risk assessment of BTEX in ambient air of a Middle Eastern City, Process Saf. Environ. Prot. 139 (2020) 98–105. https://doi.org/10.1016/J.PSEP.2020.03.019.

[5] Y. Li, C.P. Alaimo, M. Kim, N.Y. Kado, J. Peppers, J. Xue, C. Wan, P.G. Green, R. Zhang, B.M. Jenkins, C.F.A. Vogel, S. Wuertz, T.M. Young, M.J. Kleeman, Composition and Toxicity of Biogas Produced from Different Feedstocks in California, Environ. Sci. Technol. (2019). https://doi.org/10.1021/acs.est.9b03003.

[6] A.N. Baghani, A. Sorooshian, M. Heydari, R. Sheikhi, S. Golbaz, Q. Ashournejad, M. Kermani, F. Golkhorshidi, A. Barkhordari, A.J. Jafari, M. Delikhoon, A. Shahsavani, A case study of BTEX characteristics and health effects by major point sources of pollution during winter in Iran, Environ. Pollut. 247 (2019) 607–617. https://doi.org/10.1016/J.ENVPOL.2019.01.070.

[7] M.J. Milazzo, J.M. Gohlke, D.L. Gallagher, A.A. Scott, B.F. Zaitchik, L.C. Marr, Potential for city parks to reduce exposure to BTEX in air, Environ. Sci. Process. Impacts. 21 (2019) 40–50. https://doi.org/10.1039/c8em00252e.

[8] C. Peng, J.W. Lee, H.T. Sichani, J.C. Ng, Toxic effects of individual and combined effects of BTEX on Euglena gracilis, J. Hazard. Mater. 284 (2015) 10–18.

https://doi.org/10.1016/J.JHAZMAT.2014.10.024.

[9] S. Rasi, J. Läntelä, J. Rintala, Trace compounds affecting biogas energy utilisation - A review, Energy Convers. Manag. 52 (2011) 3369–3375. https://doi.org/10.1016/j.enconman.2011.07.005.

[10] E. Ryckebosch, M. Drouillon, H. Vervaeren, Techniques for transformation of biogas to biomethane, Biomass and Bioenergy. 35 (2011) 1633–1645. https://doi.org/10.1016/j.biombioe.2011.02.033.

[11] E. Santos-Clotas, A. Cabrera-Codony, E. Boada, F. Gich, R. Muñoz, M.J. Martín, Efficient removal of siloxanes and volatile organic compounds from sewage biogas by an anoxic biotrickling filter supplemented with activated carbon, Bioresour. Technol. 294 (2019) 122136. https://doi.org/10.1016/J.BIORTECH.2019.122136.

[12] W.K.E.H. Warren, A techno-economic comparison of biogas upgrading technologies in Europe, MSc Thesis. (2012) 44.

[13] I. Angelidaki, L. Xie, G. Luo, Y. Zhang, H. Oechsner, A. Lemmer, R. Munoz, P.G. Kougias, Biogas Upgrading: Current and Emerging Technologies, Biofuels Altern. Feed. Convers. Process. Prod. Liq. Gaseous Biofuels. (2019) 817–843. https://doi.org/10.1016/B978-0-12-816856-1.00033-6.

[14] O.W. Awe, Y. Zhao, A. Nzihou, D.P. Minh, N. Lyczko, A Review of Biogas Utilisation, Purification and Upgrading Technologies, Waste and Biomass Valorization. 8 (2017) 267–283. https://doi.org/10.1007/s12649-016-9826-4.

[15] S. Rasi, J. Läntelä, J. Rintala, Upgrading landfill gas using a high pressure water absorption process, Fuel. 115 (2014) 539–543. https://doi.org/10.1016/j.fuel.2013.07.082.

910 [16] C. Ma, C. Liu, X. Lu, X. Ji, Techno-economic analysis and performance comparison of
911 aqueous deep eutectic solvent and other physical absorbents for biogas upgrading,
912 Appl. Energy. 225 (2018) 437–447. https://doi.org/10.1016/j.apenergy.2018.04.112.

913 [17] I. Angelidaki, L. Treu, P. Tsapekos, G. Luo, S. Campanaro, H. Wenzel, P.G. Kougias,
914 Biogas upgrading and utilization: Current status and perspectives, Biotechnol. Adv. 36
915 (2018) 452–466. https://doi.org/10.1016/J.BIOTECHADV.2018.01.011.

916 [18] M. Scholz, B. Frank, F. Stockmeier, S. Falß, M. Wessling, Techno-economic analysis
917 of hybrid processes for biogas upgrading, Ind. Eng. Chem. Res. 52 (2013) 16929–
918 16938. https://doi.org/10.1021/ie402660s.

919 [19] N. Tazang, F. Alavi, J. Javanmardi, Estimation of solubility of BTEX, light
920 hydrocarbons and sour gases in triethylene glycol using the SAFT equation of state,
921 Phys. Chem. Res. 8 (2020) 251–266. https://doi.org/10.22036/pcr.2020.208933.1699.

922 [20] X. Xiao, B. Yan, J. Fu, X. Xiao, Absorption of gaseous toluene in aqueous solutions of
923 some kinds of fluorocarbon surfactant, J. Air Waste Manag. Assoc. 65 (2015) 90–98.
924 https://doi.org/10.1080/10962247.2014.968268.

925 [21] P. Fang, Z.J. Tang, X.B. Chen, Z.X. Tang, D.S. Chen, J.H. Huang, W.H. Zeng, C.P.
926 Cen, Experimental study on the absorption of toluene from exhaust gas by
927 paraffin/surfactant/water emulsion, J. Chem. 2016 (2016).
928 https://doi.org/10.1155/2016/9385027.

929 [22] N. HATCHER, C. JONES, R. WEILAND, Solubility of hydrocarbons and light ends in
930 amines, Pet. Technol. Q. (2013).

931 [23] C. Zhang, J. Wu, R. Wang, E. Ma, L. Wu, J. Bai, J. Wang, Study of the toluene
932 absorption capacity and mechanism of ionic liquids using COSMO-RS prediction and

933 experimental verification, Green Energy Environ. 6 (2021) 339–349.
934 https://doi.org/10.1016/J.GEE.2020.08.001.

935 [24] E. Słupek, P. Makoś, J. Gębicki, Theoretical and Economic Evaluation of Low-Cost
936 Deep Eutectic Solvents for Effective Biogas Upgrading to Bio-Methane, Energies. 13
937 (2020) 3379. https://doi.org/10.3390/en13133379.

938 [25] A.P. Abbott, G. Capper, D.L. Davies, R.K. Rasheed, V. Tambyrajah, Novel solvent
939 properties of choline chloride/urea mixtures, Chem. Commun. (2003) 70–71.
940 https://doi.org/10.1039/b210714g.

941 [26] E.L. Smith, A.P. Abbott, K.S. Ryder, Deep Eutectic Solvents (DESs) and Their
942 Applications, Chem. Rev. 114 (2014) 11060–11082.
943 https://doi.org/10.1021/cr300162p.

944 [27] Z. Ghazali, N.H. Hassan, M.A. Yarmo, T.L. Peng, R. Othaman, Immobilization of
945 choline chloride: Urea onto mesoporous silica for carbon dioxide capture, Sains
946 Malaysiana. 48 (2019) 1025–1033. https://doi.org/10.17576/jsm-2019-4805-11.

947 [28] F. Hussin, M.K. Aroua, R. Yusoff, Adsorption of CO2 on palm shell based activated
948 carbon modified by deep eutectic solvent: Breakthrough adsorption study, J. Environ.
949 Chem. Eng. 9 (2021) 105333. https://doi.org/10.1016/J.JECE.2021.105333.

950 [29] P. Makoś, G. Boczkaj, Deep eutectic solvents based highly efficient extractive
951 desulfurization of fuels – Eco-friendly approach, J. Mol. Liq. 296 (2019) 111916–
952 111927. https://doi.org/10.1016/j.molliq.2019.111916.

953 [30] S.C. Cunha, J.O. Fernandes, Extraction techniques with deep eutectic solvents, TrAC -
954 Trends Anal. Chem. 105 (2018) 225–239. https://doi.org/10.1016/j.trac.2018.05.001.

955 [31] P. Makoś, E. Słupek, A. Małachowska, Silica Gel Impregnated by Deep Eutectic

956 Solvents for Adsorptive Removal of BTEX from Gas Streams, Materials (Basel). 13
957 (2020) 1894. https://doi.org/10.3390/ma13081894.

958 [32] P. Makoś, E. Słupek, J. Gębicki, Extractive detoxification of feedstocks for the
959 production of biofuels using new hydrophobic deep eutectic solvents – Experimental
960 and theoretical studies, J. Mol. Liq. 308 (2020) 113101–113112.
961 https://doi.org/10.1016/j.molliq.2020.113101.

962 [33] S.K. Shukla, J.P. Mikkola, Intermolecular interactions upon carbon dioxide capture in
963 deep-eutectic solvents, Phys. Chem. Chem. Phys. 20 (2018) 24591–24601.
964 https://doi.org/10.1039/c8cp03724h.

965 [34] G. García, S. Aparicio, R. Ullah, M. Atilhan, Deep eutectic solvents: Physicochemical
966 properties and gas separation applications, Energy and Fuels. 29 (2015) 2616–2644.
967 https://doi.org/10.1021/ef5028873.

968 [35] L.F. Zubeir, D.J.G.P. Van Osch, M.A.A. Rocha, F. Banat, M.C. Kroon, Carbon
969 Dioxide Solubilities in Decanoic Acid-Based Hydrophobic Deep Eutectic Solvents, J.
970 Chem. Eng. Data. 63 (2018) 913–919. https://doi.org/10.1021/acs.jced.7b00534.

971 [36] Z. Ghazali, M.A. Yarmo, R. Othaman, Confinement and characterization of deep
972 eutectic solvent based on choline chloride:alcohol into nanoporous silica for CO2
973 capture, AIP Conf. Proc. 2111 (2019). https://doi.org/10.1063/1.5111262.

974 [37] Q. Luo, J. Hao, L. Wei, S. Zhai, Z. Xiao, Q. An, Protic ethanolamine hydrochloride-
975 based deep eutectic solvents for highly efficient and reversible absorption of NH3, Sep.
976 Purif. Technol. 260 (2021) 118240. https://doi.org/10.1016/j.seppur.2020.118240.

977 [38] H. Wu, M. Shen, X. Chen, G. Yu, A.A. Abdeltawab, S.M. Yakout, New absorbents for
978 hydrogen sulfide: Deep eutectic solvents of tetrabutylammonium bromide/carboxylic

acids and choline chloride/carboxylic acids, Sep. Purif. Technol. 224 (2019) 281–289. https://doi.org/10.1016/J.SEPPUR.2019.04.082.

[39] E. Słupek, P. Makoś-Chełstowska, J. Gębicki, Removal of siloxanes from model biogas by means of deep eutectic solvents in absorption process, Materials (Basel). 14 (2021) 1–20. https://doi.org/10.3390/ma14020241.

[40] P. Makoś-Chełstowska, E. Słupek, A. Kramarz, J. Gębicki, New Carvone-Based Deep Eutectic Solvents for Siloxanes Capture from Biogas, Int. J. Mol. Sci. 22 (2021) 9551–9574.

[41] E. Słupek, P. Makoś, Absorptive Desulfurization of Model Biogas Stream Using Choline Chloride-Based Deep Eutectic Solvents, Sustainability. 12 (2020) 1619–1635. https://doi.org/10.3390/su12041619.

[42] P. Makoś-Chełstowska, E. Słupek, J. Gębicki, Deep eutectic solvents – based green absorbents for effective volatile organochlorine compounds removal from biogas, Green Chem. (2021). https://doi.org/10.1039/d1gc01735g.

[43] L. Moura, T. Moufawad, M. Ferreira, H. Bricout, S. Tilloy, E. Monflier, M.F. Costa Gomes, D. Landy, S. Fourmentin, Deep eutectic solvents as green absorbents of volatile organic pollutants, Environ. Chem. Lett. 15 (2017) 747–753. https://doi.org/10.1007/s10311-017-0654-y.

[44] E. Słupek, P. Makoś, J.Gębicki, Deodorization of model biogas by means of novel non-ionic deep eutectic solvent, Arch. Environ. Prot. 46 (2020) 41–46. https://doi.org/10.24425/aep.2020.132524.

[45] B. Szulczyński, P. Rybarczyk, J. Gębicki, Monitoring of n-butanol vapors biofiltration process using an electronic nose combined with calibration models, Monatshefte Fur

Chemie. 149 (2018) 1693–1699. https://doi.org/10.1007/s00706-018-2243-6.

[46] P. Rybarczyk, B. Szulczyński, J. Gebicki, Simultaneous removal of hexane and ethanol from air in a biotrickling filter-process performance and monitoring using electronic nose, Sustain. 12 (2020). https://doi.org/10.3390/su12010387.

[47] R. López, I.O. Cabeza, I. Giráldez, M.J. Díaz, Biofiltration of composting gases using different municipal solid waste-pruning residue composts: Monitoring by using an electronic nose, Bioresour. Technol. 102 (2011) 7984–7993. https://doi.org/10.1016/J.BIORTECH.2011.05.085.

[48] I.O. Cabeza, R. López, I. Giraldez, R.M. Stuetz, M.J. Díaz, Biofiltration of α-pinene vapours using municipal solid waste (MSW) – Pruning residues (P) composts as packing materials, Chem. Eng. J. 233 (2013) 149–158. https://doi.org/10.1016/J.CEJ.2013.08.032.

[49] A. Romero-Flores, L.L. McConnell, C.J. Hapeman, M. Ramirez, A. Torrents, Evaluation of an electronic nose for odorant and process monitoring of alkaline-stabilized biosolids production, Chemosphere. 186 (2017) 151–159. https://doi.org/10.1016/J.CHEMOSPHERE.2017.07.135.

[50] D. Dobrzyniewski, B. Szulczyński, T. Dymerski, J. Gębicki, Development of gas sensor array for methane reforming process monitoring, Sensors. 21 (2021) 1–15. https://doi.org/10.3390/s21154983.

[51] T.C. Pearce, J.W. Gardner, S. Friel, P.N. Bartlett, N. Blair, Electronic nose for monitoring the flavour of beers, Analyst. 4 (1993) 371–377. https://doi.org/10.1039/AN9931800371.

[52] S. Spichiger, U.E. Spichiger-Keller, Process monitoring with disposable chemical

sensors fit in the framework of process analysis technology (PAT) for innovative pharmaceutical development and quality assurance, Chimia (Aarau). 64 (2010) 803–807. https://doi.org/10.2533/chimia.2010.803.

[53] X.S. Chai, J.B. Falabella, A.S. Teja, A relative headspace method for Henry's constants of volatile organic compounds, Fluid Phase Equilib. 231 (2005) 239–245. https://doi.org/10.1016/J.FLUID.2005.02.006.

[54] P. Makoś-Chełstowska, E. Słupek, A. Małachowska, Superhydrophobic sponges based on green deep eutectic solvents for spill oil removal from water, J. Hazard. Mater. 425 (2022). https://doi.org/10.1016/j.jhazmat.2021.127972.

[55] M.W.A. Lawal, P. Stephenson, J. Sidders, C. Ramshaw, H. Yeung, Post-combustion CO 2 Capture with Chemical Absorption : A State-of-the-art Review, Chem. Eng. Res. Des. 89 (2011) 1609–1624.

[56] C.C. Chen, Y.H. Huang, J.Y. Fang, Hydrophobic deep eutectic solvents as green absorbents for hydrophilic VOC elimination, J. Hazard. Mater. 424 (2022) 127366. https://doi.org/10.1016/J.JHAZMAT.2021.127366.

[57] W. Wang, Y. Zhang, W. Liu, Bioinspired fabrication of high strength hydrogels from non-covalent interactions, Prog. Polym. Sci. 71 (2017) 1–25. https://doi.org/10.1016/J.PROGPOLYMSCI.2017.04.001.

[58] T. Brouwer, S.R.A. Kersten, G. Bargeman, B. Schuur, trends in solvent impact on infinite dilution activity coefficients of solutes reviewed and visualized using an algorithm to support selection of solvents for greener fluid separations, Sep. Purif. Technol. 272 (2021) 118727. https://doi.org/10.1016/J.SEPPUR.2021.118727.

[59] B.D. Ribeiro, C. Florindo, L.C. Iff, M.A.Z. Coelho, I.M. Marrucho, Menthol-based

eutectic mixtures: Hydrophobic low viscosity solvents, ACS Sustain. Chem. Eng. 3 (2015) 2469–2477. https://doi.org/10.1021/acssuschemeng.5b00532.

[60] C. Florindo, F.S. Oliveira, L.P.N. Rebelo, A.M. Fernandes, I.M. Marrucho, Insights into the synthesis and properties of deep eutectic solvents based on cholinium chloride and carboxylic acids, ACS Sustain. Chem. Eng. 2 (2014) 2416–2425. https://doi.org/10.1021/sc500439w.

[61] F. Chemat, H. Anjum, A.M. Shariff, P. Kumar, T. Murugesan, Thermal and physical properties of (Choline chloride + urea + l-arginine) deep eutectic solvents, J. Mol. Liq. 218 (2016) 301–308. https://doi.org/10.1016/J.MOLLIQ.2016.02.062.

[62] A. Hayyan, F.S. Mjalli, I.M. Alnashef, T. Al-Wahaibi, Y.M. Al-Wahaibi, M.A. Hashim, Fruit sugar-based deep eutectic solvents and their physical properties, Thermochim. Acta. 541 (2012) 70–75. https://doi.org/10.1016/j.tca.2012.04.030.

[63] P. Makoś, E. Słupek, J. Gębicki, Hydrophobic deep eutectic solvents in microextraction techniques–A review, Microchem. J. 152 (2020). https://doi.org/10.1016/j.microc.2019.104384.

[64] P. Makoś-Chełstowska, E. Słupek, A. Małachowska, Superhydrophobic sponges based on green deep eutectic solvents for spill oil removal from water, J. Hazard. Mater. 425 (2022) 127972. https://doi.org/10.1016/J.JHAZMAT.2021.127972.

[65] C. Fan, T. Sebbah, Y. Liu, X. Cao, Terpenoid-capric acid based natural deep eutectic solvent: Insight into the nature of low viscosity, Clean. Eng. Technol. 3 (2021) 100116. https://doi.org/10.1016/j.clet.2021.100116.

[66] R. Haghbakhsh, K. Parvaneh, S. Raeissi, A. Shariati, A general viscosity model for deep eutectic solvents: The free volume theory coupled with association equations of

state, Fluid Phase Equilib. 470 (2018) 193–202. https://doi.org/10.1016/j.fluid.2017.08.024.

[67] E. Jiménez, M. Cabanas, L. Segade, S. García-Garabal, H. Casas, Excess volume, changes of refractive index and surface tension of binary 1,2-ethanediol + 1-propanol or 1-butanol mixtures at several temperatures, Fluid Phase Equilib. 180 (2001) 151–164. https://doi.org/10.1016/S0378-3812(00)00519-7.

[68] Y. Chen, W. Chen, L. Fu, Y. Yang, Y. Wang, X. Hu, F. Wang, T. Mu, Surface Tension of 50 Deep Eutectic Solvents: Effect of Hydrogen-Bonding Donors, Hydrogen-Bonding Acceptors, Other Solvents, and Temperature, Ind. Eng. Chem. Res. 58 (2019) 12741–12750. https://doi.org/10.1021/acs.iecr.9b00867.

[69] K. Shahbaz, F.S. Mjalli, M.A. Hashim, I.M. AlNashef, Prediction of the surface tension of deep eutectic solvents, Fluid Phase Equilib. 319 (2012) 48–54. https://doi.org/10.1016/j.fluid.2012.01.025.

[70] K.A. Kurnia, M.I.A. Mutalib, Z. Man, M.A. Bustam, Density and Surface Tension of Ionic Liquids [H2N–C2mim][PF6] and [H2N–C3mim][PF6], J. Chem. Eng. Data. (2012) 17025–17036.

[71] A.P. Abbott, R.C. Harris, K.S. Ryder, C. D'Agostino, L.F. Gladden, M.D. Mantle, Glycerol eutectics as sustainable solvent systems, Green Chem. 13 (2011) 82–90. https://doi.org/10.1039/c0gc00395f.

[72] F.S. Mjalli, J. Naser, B. Jibril, V. Alizadeh, Z. Gano, Tetrabutylammonium chloride based ionic liquid analogues and their physical properties, J. Chem. Eng. Data. 59 (2014) 2242–2251. https://doi.org/10.1021/je5002126.

[73] P. Makoś-Chełstowska, E. Słupek, J. Gębicki, Deep eutectic solvent-based green

absorbents for the effective removal of volatile organochlorine compounds from biogas, Green Chem. (2021) 4814–4827. https://doi.org/10.1039/d1gc01735g.

[74] J.I. Salazar Gómez, H. Lohmann, J. Krassowski, Determination of volatile organic compounds from biowaste and co-fermentation biogas plants by single-sorbent adsorption, Chemosphere. 153 (2016) 48–57. https://doi.org/10.1016/j.chemosphere.2016.02.128.

[75] M.D. López, M.J. Pascual-Villalobos, Mode of inhibition of acetylcholinesterase by monoterpenoids and implications for pest control, Ind. Crops Prod. 31 (2010) 284–288. https://doi.org/10.1016/j.indcrop.2009.11.005.

[76] C.C. Chen, Y.H. Huang, S.M. Hung, C. Chen, C.W. Lin, H.H. Yang, Hydrophobic deep eutectic solvents as attractive media for low-concentration hydrophobic VOC capture, Chem. Eng. J. 424 (2021) 130420. https://doi.org/10.1016/j.cej.2021.130420.

[77] S. Tsuzuki, A. Fujii, Nature and physical origin of CH/p interaction: significant difference from conventional hydrogen bonds, Phys. Chem. Chem. Phys. 10 (2008) 2581–2583. https://doi.org/10.1039/b805489b.

[78] E.M. Cabaleiro-Lago, J. Rodríguez-Otero, On the Nature of σ-σ, σ-π, and π-π Stacking in Extended Systems, ACS Omega. 3 (2018) 9348–9359. https://doi.org/10.1021/acsomega.8b01339.

[79] A. Janusz-Cygan, J. Jaschik, M. Tańczyk, Upgrading biogas from small agricultural sources into biomethane by membrane separation, Membranes (Basel). 11 (2021) 10–14. https://doi.org/10.3390/membranes11120938.

[80] T. Altamash, A.I. Amhamed, S. Aparicio, M. Atilhan, Combined Experimental and Theoretical Study on High Pressure Methane Solubility in Natural Deep Eutectic

Solvents, Ind. Eng. Chem. Res. 58 (2019) 8097–8111. https://doi.org/10.1021/acs.iecr.9b00702.

[81] J. Han, C. Dai, G. Yu, Z. Lei, Parameterization of COSMO-RS model for ionic liquids, Green Energy Environ. 3 (2018) 247–265. https://doi.org/https://doi.org/10.1016/j.gee.2018.01.001.

[82] V. Muresan, M.L. Unguresan, C. Varodi, J.Z. Szucs-Balazs, Temperature influence over the absorption process of CO2 in octane, Proc. - 2015 8th Rom. Tier 2 Fed. Grid, Cloud High Perform. Comput. Sci. ROLCG 2015. (2015) 1–5. https://doi.org/10.1109/ROLCG.2015.7367420.

[83] T. Kvist, N. Aryal, Methane loss from commercially operating biogas upgrading plants, Waste Manag. 87 (2019) 295–300.

[84] A. Universite, Development of a hybrid process , Membrane-Ionic Liquid (ILM), for gas treatment, (2020).

[85] V.C. Ramos, W. Han, K.L. Yeung, A comparative study between ionic liquid coating and counterparts in bulk for toluene absorption, Green Chem. Eng. 1 (2020) 147–154. https://doi.org/10.1016/j.gce.2020.10.008.